

Modeling the response of the oceanic Si inventory to perturbation, and consequences for atmospheric CO₂

Andy J. Ridgwell¹

School of Environmental Sciences, University of East Anglia, Norwich, UK

Tyndall Centre for Climate Change Research, University of East Anglia, Norwich, UK

Andrew J. Watson

School of Environmental Sciences, University of East Anglia, Norwich, UK

David E. Archer

Department of the Geophysical Sciences, University of Chicago, Chicago, Illinois, USA

Received 31 January 2002; revised 31 May 2002; accepted 10 June 2002; published 5 November 2002.

[1] It has been suggested that much of the observed glacial-interglacial variability in the atmospheric mixing ratio of CO₂ ($x\text{CO}_2$) could potentially be driven by a perturbation of the marine Si cycle. To date, only relatively simple steady-state analysis has been made of this hypothesis. In this study, we develop a description of the ocean carbon cycle, incorporating novel descriptions for the recycling of Si, both within the water column and in deep-sea sediments. A high degree of computational efficiency enables model integrations over multiple glacial-interglacial cycles, driven by a time-varying input of dissolved Si to the ocean. Due to the long time constant (~ 23 ka) of atmospheric $x\text{CO}_2$ response to perturbation in Si supply and the highly nonlinear nature of opal preservation in deep-sea sediments, we find that reduction in the deposition rate of aeolian silicates at the surface ocean can explain little (< 3 ppm) of the rapid ~ 90 ppm rise in atmospheric $x\text{CO}_2$ observed at glacial termination. However, increased Si supply has the potential to make an important contribution to the decline in atmospheric $x\text{CO}_2$ associated with the much slower transition from interglacial to full glacial conditions. INDEX

TERMS: 3022 Marine Geology and Geophysics: Marine sediments—processes and transport; 1615 Global Change: Biogeochemical processes (4805); 4806 Oceanography: Biological and Chemical: Carbon cycling; 4815 Oceanography: Biological and Chemical: Ecosystems, structure and dynamics; KEYWORDS: marine silica cycle, carbon cycle, glacial, opal, dust

Citation: Ridgwell, A. J., A. J. Watson, and D. E. Archer, Modeling the response of the oceanic Si inventory to perturbation, and consequences for atmospheric CO₂, *Global Biogeochem. Cycles*, 16(4), 1071, doi:10.1029/2002GB001877, 2002.

1. Introduction

[2] Dissolved silica (silicic acid, or H₄SiO₄) is ubiquitously present in the intermediate and deep ocean [Tréguer *et al.*, 1995], and as with other phytoplankton nutrients, is often virtually absent from the surface ocean [Conkright *et al.*, 1994]. However, the role played by silicic acid in the global carbon cycle appears to be somewhat subtler. When either phosphate, nitrate, or iron is in insufficient supply, it tends to restrict virtually all phytoplankton growth and with it, the export of particulate organic carbon (POC) from the surface ocean. Silicic acid, in contrast, is vital only for siliceous phytoplankton (diatoms) that rely on the construction of opaline frustules for cellular support and protection

[Ragueneau *et al.*, 2000]. If conditions are otherwise favorable for growth, and H₄SiO₄ is plentiful, diatoms out-compete most other (nonsiliceous) phytoplankton species and dominate the ecosystem [Aksnes *et al.*, 1994; Egge, 1998; Egge and Aksnes, 1992]. Where the availability of H₄SiO₄ is restricted, diatoms tend to play a less important role. In this way, the supply of silicic acid to the surface ocean could be considered as a regulator of ecosystem composition [Egge and Aksnes, 1992; Officer and Ryther, 1980; Ragueneau *et al.*, 2000].

[3] While diatoms (together with their zooplankton equivalent – radiolarians) are responsible for all of the biogenic opal production in the open ocean, it is only among the nonsiliceous phytoplankton species such as coccolithophorids (together with their zooplankton equivalent – foraminifera) that producers of calcium carbonate (CaCO₃) are found. Changes in ecosystem structure, specifically the balance between siliceous and nonsiliceous phytoplankton, may then affect the ratio of CaCO₃ to POC exported from

¹Now at Department of Earth Sciences, University of California, Riverside, California 92521, USA.

the euphotic zone [Ragueneau *et al.*, 2000] (assuming that total POC export is relatively unaffected). The CaCO_3 :POC “rain ratio” reaching the ocean floor exerts an important influence upon the preservation and burial of CaCO_3 in sediments [Archer, 1991, 1996]. Changes in global CaCO_3 burial rates, in turn, affect ocean chemistry, and with it, the atmospheric mixing ratio of CO_2 ($x\text{CO}_2$). Indeed, model studies have demonstrated that it is possible to account for the difference in atmospheric $x\text{CO}_2$ between interglacial and glacial times (~ 90 ppm) [Petit *et al.*, 1999] through a 40% reduction in this ratio [Archer and Maier-Reimer, 1994]. In light of this mechanism, it has recently been suggested that changes in the supply of dissolved silica to the ocean might account for the observed glacial-interglacial variability in $x\text{CO}_2$. Perturbation of Si supply could be driven by changes in the deposition of mineral aerosol (“dust”) to the surface ocean [Harrison, 2000] and/or changes in terrestrial weathering rates (and thus riverine supply) [Tréguer and Pondaven, 2000]. However, the dynamical (i.e., nonsteady state) response of the global silica cycle (and thus of atmospheric $x\text{CO}_2$) to perturbation has not been studied previously.

[4] Here, we present a model of the ocean carbon cycle, designed to be numerically efficient and thus afford easy access to glacial-interglacial time scales. New parameterizations are developed for two critical Si recycling processes within the system – remineralization of biogenic opal in deep-sea sediments and in the water column. This model is employed to investigate the response of the marine Si cycle to perturbation of external (dissolved) Si input, and thus assess recent hypotheses surrounding the role that such perturbations may have played in explaining the variability in atmospheric $x\text{CO}_2$ observed over the course of the late Quaternary.

2. Recycling of Si From Biogenic Opal

[5] On time scales of tens of thousands of years (ka), Si is lost from the ocean through the burial of biogenic opal in marine sediments and replenished via input from sources such as dust, rivers, and hydrothermal alteration [Tréguer *et al.*, 1995]. It is the magnitude of this loss rate relative to the total oceanic Si inventory that determines the time scale of response (of the Si inventory) to any perturbation of Si supply. However, before it can be lost through sedimentary burial, biogenic opal formed within the euphotic zone (the uppermost sunlit layer the ocean) may be recycled back to the dissolved (H_4SiO_4) form in any one of three primary regimes (Figure 1) i.e., the euphotic zone, the water column of the ocean interior, and in sediments lying on the ocean floor. As a result, processes in all three regimes play a role in determining the final loss rate. In this study, we focus on the latter two regimes, and in particular on the sediments, because it is here that the greatest fractional dissolution of biogenic opal and return of H_4SiO_4 to the ocean occurs, and thus the most important control is exerted.

2.1. Sedimentary Opal Diagenesis

[6] Despite the importance of opal burial in deep-sea sediments, both to the operation of the global carbon cycle in general, and to the interpretation of paleoceanographic

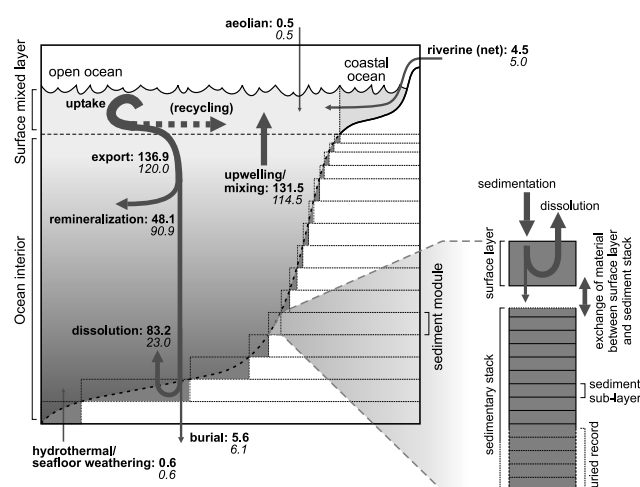


Figure 1. Schematic of the global ocean biogeochemical cycling of Si, together with the structure of the sediment system. Arrows indicate the flow of Si (as either silicic acid or biogenic opal), with values (in units of Tmol Si a^{-1}) of these fluxes in the model at steady state shown in bold, and contrasted with those shown in the work of Tréguer *et al.* [1995] (italics). The riverine input flux is quoted “less” removal in coastal/shelf zones (i.e., as the net input to the “open ocean”). The dotted arrow indicates recycling within the euphotic zone, not resolved in the simple export production scheme employed here. Indicated is the distribution of the 15 sediment modules (which together span 100–6000 m depth range of ocean) associated with each oceanic region in the zonally averaged representation of ocean circulation (see Figure 6). Each of these sediment modules is composed of a 10 cm thick surface layer (in which diagenesis is assumed to take place), underlain by a stack of (1 cm thick) storage or sediment compositional “memory” layers. See color version of this figure at back of this issue.

proxies of past climatic change [Charles *et al.*, 1991; Kumar *et al.*, 1995; Mortlock *et al.*, 1991; Pondaven *et al.*, 2000], the factors determining opal preservation are poorly understood [Archer *et al.*, 1993; Boyle, 1998; Ragueneau *et al.*, 2000]. A new description of sedimentary opal diagenesis is presented in this article. This is developed using empirical functional relationships derived from recent observations and from laboratory analyses of opal dissolution and thermodynamics [Rabouille *et al.*, 1997; VanCappellen and Qiu, 1997a, 1997b].

2.1.1. A Model for Sedimentary Opal Diagenesis

[7] The representation of opal dissolution within deep-sea sediments is simplified by considering activity only in the uppermost 10 cm (see Figure 1). This appears justified on the basis of little net diffusion of H_4SiO_4 observed below this depth [Rabouille *et al.*, 1997; Sayles *et al.*, 1996; VanBennekom *et al.*, 1988]. A further simplifying assumption is made - that of constant opal concentration with depth in the sediments, also consistent with observations [Rabouille *et al.*, 1997; Schluter and Sauter, 2000; VanBennekom *et al.*, 1988]. Porosity in the sediments is assumed to decrease from $0.95 \text{ cm}^3 \text{ cm}^{-3}$ at the surface to $0.7 \text{ cm}^3 \text{ cm}^{-3}$ at depth [Ridgwell, 2001], with bioturbational mixing rates following

the studies by *Archer* [1991]. The system is vertically discretized into 0.2 cm thick layers, and solved on a forward-time finite-difference basis. Since the relaxation time of solute composition is several orders of magnitude faster than for solids [*Rabouille and Gaillard*, 1990], pore-water concentrations are solved for in isolation. Steady state is assumed to have been reached when the dissolution flux across the sediment-water interface changes by less than 0.001% between time steps (2×10^6 s). The two components of the diffusion-reaction system are defined in the following sections.

2.1.1.1. Diffusion of H_4SiO_4

[8] Correcting for tortuosity [*Ullman and Aller*, 1982], the in situ diffusivity of H_4SiO_4 at depth z in the sediment ($D_{\text{sed}(z)}$) is described by

$$D_{\text{sed}(z)} = \left(\phi_{(z)}\right)^{(n-1)} D_{\text{SW}} \quad (1)$$

where D_{SW} is the molecular diffusivity of H_4SiO_4 in free seawater, $\phi_{(z)}$ is the porosity at depth z , and n is a correlation factor, typically taking a value of 2.5 for deep-sea sediments [*Hensen et al.*, 1998; *Ullman and Aller*, 1982]. D_{SW} has a value of $4.59 \times 10^{-6} \text{ cm}^2 \text{ s}^{-1}$ at 0°C , and is adjusted for ambient bottom-water temperature (T_{SW} , in Kelvin) following *Hensen et al.*

$$D_{\text{SW}} = 4.59 \times 10^{-6} + 1.74 \times 10^{-7}(T_{\text{SW}} - 273.15) \quad (2)$$

[9] When compared with the molecular diffusion of H_4SiO_4 , aqueous transport due to bioturbation and advection (resulting from sediment accumulation) is not significant [*Schink et al.*, 1975] and is therefore not taken into account.

2.1.1.2. Dissolution of Biogenic Opal

[10] The dissolution rate of opal (in units of $\text{mol Si cm}^{-3} \text{ a}^{-1}$) at depth z in the sediment is defined as

$$R_{(z)}^{\text{opal}} = k_{(z)}^{\text{opal}} \rho^{\text{opal}} [1 - \phi_{(z)}] c_{(z)}^{\text{opal}} \quad (3)$$

where $k_{(z)}^{\text{opal}}$ is a dissolution rate constant (a^{-1}), ρ^{opal} is the density of opal (mol cm^{-3}), $\phi_{(z)}$ is sediment porosity ($\text{cm}^3 \text{ cm}^{-3}$), and $c_{(z)}^{\text{opal}}$ is the fraction of opal ($\text{cm}^3 \text{ cm}^{-3}$) as a proportion of sediment solids. Dissolution is typically assumed to proceed as a linear function of the degree of undersaturation [*Archer et al.*, 1993, 2000b; *Rabouille and Gaillard*, 1990; *Rabouille et al.*, 1997; *Schink et al.*, 1975]

$$k_{(z)}^{\text{opal}} = a u_{(z)}^{\text{opal}} \quad (4)$$

where a is a constant and $u_{(z)}^{\text{opal}}$ is the degree of local pore-water undersaturation with respect to the solid phase

$$u_{(z)}^{\text{opal}} = \frac{[\text{H}_4\text{SiO}_4]_{\text{eq}(z)}^{\text{opal}} - [\text{H}_4\text{SiO}_4]_{(z)}}{[\text{H}_4\text{SiO}_4]_{\text{eq}(z)}^{\text{opal}}} \quad (5)$$

with $[\text{H}_4\text{SiO}_4]_{(z)}$ being the pore water concentration of silicic acid and $[\text{H}_4\text{SiO}_4]_{\text{eq}(z)}^{\text{opal}}$ being the equilibrium (saturation) concentration (with respect to the solid phase). The value of $[\text{H}_4\text{SiO}_4]_{\text{eq}(z)}^{\text{opal}}$ can be estimated empirically [*VanCappellen and Qiu*, 1997a]

$$\log_{10} \left([\text{H}_4\text{SiO}_4]_{\text{eq}(z)}^{\text{opal}} \right) = 6.44 - \frac{968}{T} \quad (6)$$

where T is the absolute temperature. Although some degree of dependence of $[\text{H}_4\text{SiO}_4]_{\text{eq}(z)}^{\text{opal}}$ on pH has also been

observed [*VanCappellen and Qiu*, 1997a], errors arising from the omission of this effect are unlikely to be more than about 5% (of $[\text{H}_4\text{SiO}_4]_{\text{eq}(z)}^{\text{opal}}$) under typical ambient conditions.

[11] The dissolution of opal may not be linear in $u_{(z)}^{\text{opal}}$, however [*Rickert et al.*, 2002]. *VanCappellen and Qiu* [1997b] found a significant deviation from a simple linear relationship as u^{opal} approached unity (Figure 2), which can be approximated by

$$R^{\text{opal}} = 0.16 \left(1 + \frac{T}{15} \right) u^{\text{opal}} + 0.55 \left(\left(1 + \frac{T}{400} \right)^4 u^{\text{opal}} \right)^{9.25} \quad (7)$$

where R^{opal} is the dissolution rate of opal (in units of $\text{nmol Si s}^{-1} \text{ g}^{-1} \text{ SiO}_2$) and T is the temperature ($^\circ\text{C}$). Although the form of this function is somewhat ad hoc, it is empirically consistent with available data over a range in T and u^{opal} , which spans typical abyssal conditions. The function is also characterized by a Q_{10} value of 2.3, consistent with experimental observations [*Kamatani*, 1982]. A scaling factor $\eta_{1(z)}^{\text{opal}}$ (accounting for the relative change in dissolution rate due to any deviation in ambient temperature from 0°C and in u^{opal} from completely undersaturating conditions) is derived by normalizing equation (7) to a value of unity at $T = 0^\circ\text{C}$ and $u_{(z)}^{\text{opal}} = 1.0$

$$\eta_{1(z)}^{\text{opal}} = 0.225 \left(1 + \frac{T}{15} \right) u_{(z)}^{\text{opal}} + 0.775 \left(\left(1 + \frac{T}{400} \right)^4 u_{(z)}^{\text{opal}} \right)^{9.25} \quad (8)$$

[12] The early diagenetic alteration of opal appears to have an additional effect on dissolution rates, with the rate constant exhibiting an inverse correlation with depth in the sediment [*VanCappellen and Qiu*, 1997b] (Figure 3). This can be approximated by

$$R^{\text{opal}} = 0.068 + 0.194e^{\left(\frac{-z}{70}\right)} \quad (9)$$

[13] Normalizing equation (9) to a value of unity at the sediment surface gives a second scaling factor

$$\eta_{2(z)}^{\text{opal}} = 0.26 + 0.74e^{\left(\frac{-z}{70}\right)} \quad (10)$$

[14] The introduction of $\eta_{2(z)}^{\text{opal}}$ is analogous to the decrease in kinetic ‘‘constant’’ with depth employed by *Rabouille et al.* [1997].

[15] Solubility also appears to be affected by diagenetic alteration within the sediments. The presence of Al contained within the silica structure of biogenic opal is associated with markedly lower solubility [*Dixit et al.*, 2001; *Rickert et al.*, 2002; *VanBennekom et al.*, 1988; *Willey*, 1975]. This is consistent with observations made by *VanCappellen and Qiu* [1997a] regarding the attainment of an asymptotic concentration of pore-water silicic acid with increasing depth in the sediment ($[\text{H}_4\text{SiO}_4]_{\text{asym}}$). They found that $[\text{H}_4\text{SiO}_4]_{\text{asym}}$ correlates with the mass ratio of detrital material to opal, leading them to suggest that the solubility decrease might be due to interstitial incorporation of Al in the surface layer during a process of continuous dissolution/recrystallization. This reduction in $[\text{H}_4\text{SiO}_4]_{\text{asym}}$

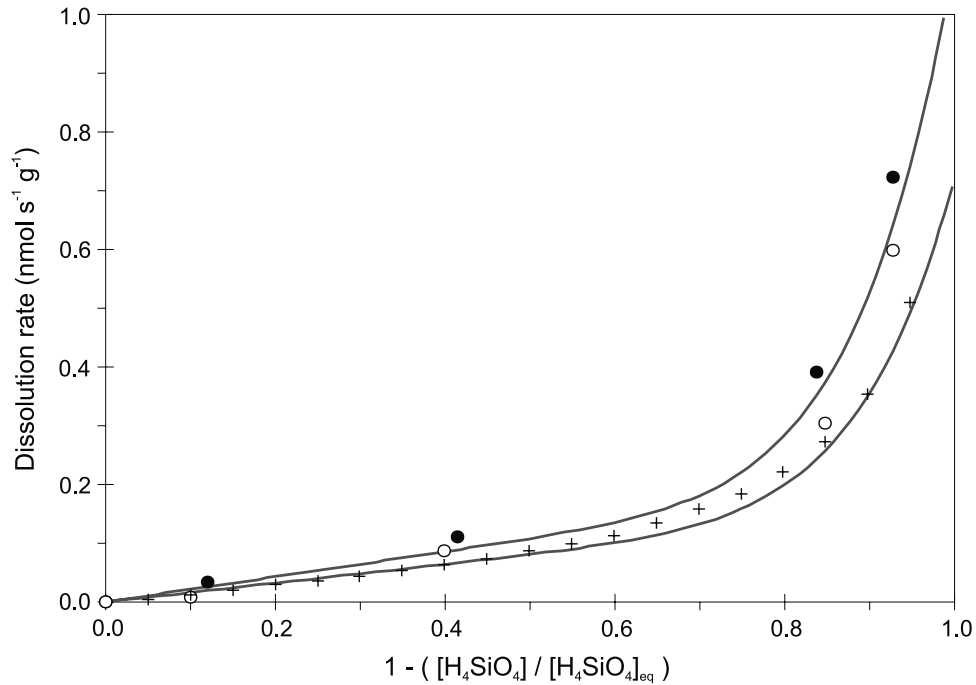


Figure 2. Opal dissolution rate as a function of degree of undersaturation with respect to the solid phase. Directly measured (at 5°C) dissolution rates are shown as filled (for core KYB05) and unfilled (KTB06) circles, respectively, together with estimated (at 0°C) dissolution rates marked by crosses [VanCappellen and Qiu, 1997b]. Calculated dissolution rates using equation (7) are shown for temperatures of 5°C (top line) and 0°C (bottom line).

with an increasing proportion of detrital material can be approximated by (Figure 4)

$$[H_4SiO_4]_{asym} = 895 - \left(5528 \frac{c^{detrital}}{c^{opal}} \right)^{0.58} \quad (11)$$

where $c^{detrital}$ and c^{opal} are the relative abundances (wt%) of detrital material and opal in the sediment, respectively. Although the highest sediment core %detrital/%opal ratio measured by VanCappellen and Qiu [1997a] was 4.8, which

corresponds to a suppression of $[H_4SiO_4]_{asym}$ to $\sim 520 \mu\text{mol kg}^{-1}$, values of $[H_4SiO_4]_{asym}$ as low as $150\text{--}300 \mu\text{mol kg}^{-1}$ have been observed in opal-poor cores [Archer et al., 1993; Martin et al., 1991; McManus et al., 1995]. The observed relationship is therefore extrapolated to a maximum %detrital/%opal ratio of 15, producing a potential minimum $[H_4SiO_4]_{asym}$ value of $\sim 180 \mu\text{mol kg}^{-1}$. A dependence of asymptotic silicic acid concentration on sediment composi-

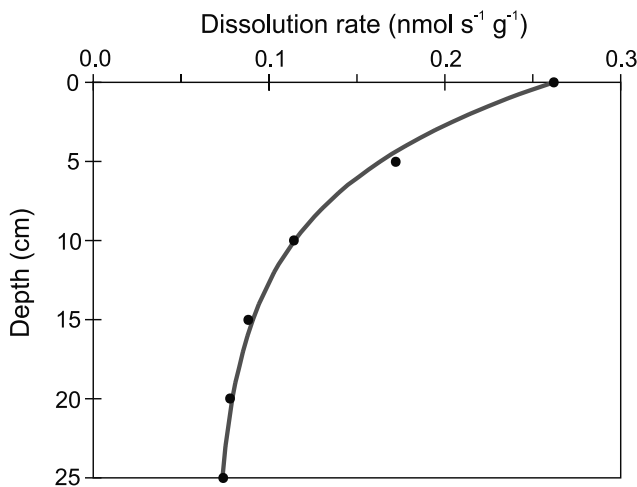


Figure 3. Down core decrease in opal dissolution rate (at half-saturation); observed data (filled circles) from VanCappellen and Qiu [1997b] along with empirical fit (9).

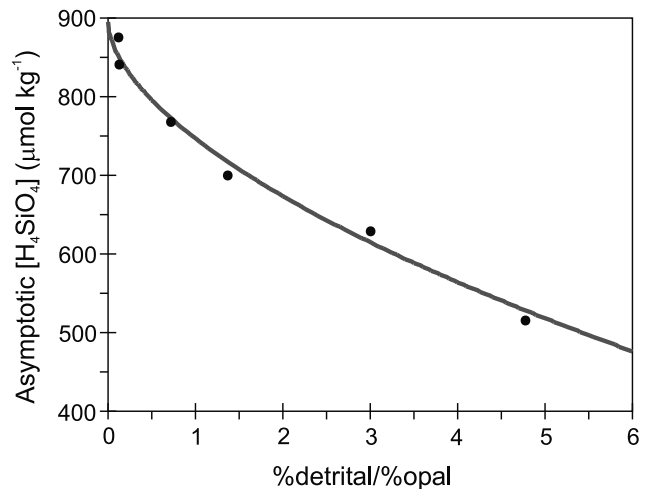


Figure 4. Dependence of down core asymptotic silicic acid concentrations on the ratio of detrital to opal sediment content; observed data (filled circles) from VanCappellen and Qiu [1997a] along with model fit (11).

Table 1. Details of Sediment Core Observations^a Together With Opal Model Predictions

Core ID	Opal, wt%	Detrital, wt%	wt% _{detrital} wt% _{opal}	[H ₄ SiO ₄] _{asym} ^a μmol kg ⁻¹	$f_{\text{dis}}^{\text{opal}}$, ^a μmol cm ⁻² a ⁻¹	[H ₄ SiO ₄] _{asym} ^b μmol kg ⁻¹	$f_{\text{dis}}^{\text{opal}}$, ^b μmol cm ⁻² a ⁻¹	k_0^{opal} , ^b a ⁻¹
KTB05	75.5	9.2	0.12	875	132.0	835	146.3	0.293
KTB06	86.3	10.8	0.13	841	203.0	834	154.0	0.288
KTB11	36.7	26.5	0.72	768	66.0	761	65.4	0.119
KTB19	38.0	52.2	1.37	700	53.5 ^c	709	55.7	0.093
KTB26	17.5	53.3	3.05	629	31.0	608	30.3	0.074
KTB28	15.8	75.5	4.78	515	24.0	526	23.9	0.067

^aRabouille *et al.* [1997].^bPredictions using the complete opal sedimentary digenesis model (equations (14) and (15)).^cEstimated.

tion is accountable on a purely kinetic basis [Rabouille *et al.*, 1997]. However, in order to reduce the number of free parameters in the model, the simplifying assumption is made that the equilibrium saturation state of opal ($[H_4SiO_4]_{\text{eq}(z)}^{\text{opal}}$) has the same functional relationship to detrital content that is observed for the asymptotic silicic acid concentration at depth in the sediments [VanCappellen and Qiu, 1997a]. A solubility reduction factor (γ_{Al}) to account for Al-inhibition is defined as

$$\gamma_{\text{Al}} = 0.2 \frac{c^{\text{detrital}}}{c^{\text{opal}}} > 15 \quad (12a)$$

$$\gamma_{\text{Al}} = 1.0 - \left(0.045 \frac{c^{\text{detrital}}}{c^{\text{opal}}}\right)^{0.58} \frac{c^{\text{detrital}}}{c^{\text{opal}}} \leq 15 \quad (12b)$$

[16] Applying this factor to modify $[H_4SiO_4]_{\text{eq}(z)}^{\text{opal}}$ equation (6) gives

$$[H_4SiO_4]_{\text{eq}(z)}^{\text{opal}} = \gamma_{\text{Al}} 10^{\left(\frac{6.44968}{T(z)}\right)} \quad (13)$$

[17] A full description for the dissolution rate of opal within the sediments can now be written as

$$R_{(z)}^{\text{opal}} = \eta_{1(z)}^{\text{opal}} \eta_{2(z)}^{\text{opal}} k_0^{\text{opal}} \rho^{\text{opal}} [1 - \phi_{(z)}] c_{(z)}^{\text{opal}} \quad (14)$$

where k_0^{opal} is the dissolution rate constant (a⁻¹) for “fresh” opaline material delivered to the sediment surface (i.e., in a diagenetically unaltered state) and with respect to a completely under-saturated environment at a temperature of 0°C.

[18] Published estimates for the dissolution rate constant of opal vary widely. A model fitting study based on a series of Antarctic cores gave values at the sediment surface in the range of 0.016–0.315 a⁻¹ [Rabouille *et al.*, 1997]. Schink *et al.* [1975] adopted a value of 0.032 a⁻¹, but noted that experimental determinations often give much higher values – upwards of 0.063–0.252 a⁻¹. A further complication arises because these estimates are potentially compromised by the assumption of linear kinetics.

[19] We estimate possible values for k_0^{opal} by fitting the opal dissolution flux across the sediment-water interface ($f_{\text{dis}}^{\text{opal}}$) for each of the cores detailed in Table 1. Model runs were informed by observed opal and detrital content [Rabouille *et al.*, 1997] and assuming a bottom-water H₄SiO₄ concentration of 145 μmol kg⁻¹, typical of the regions of the Southern Ocean from which the cores were recovered [Conkright *et al.*, 1994]. Laboratory analyses on these cores were carried out at relatively elevated temper-

atures (2°–4°C) [Rabouille *et al.*, 1997] compared to the abyssal Southern Ocean, making the likelihood of post-recovery distortion of the $[H_4SiO_4]$ profile likely [Martin *et al.*, 1991; McManus *et al.*, 1995]. An ambient temperature of 3.5°C is thus assumed, which then enables good agreement between observed [Rabouille *et al.*, 1997] and predicted (equation (6)) asymptotic power water H₄SiO₄ concentrations to be reached. However, despite taking into account the differing oceanic and sedimentary conditions, the value of base rate constant (k_0^{opal}) required to reproduce the flux estimates of Rabouille *et al.* [1997] still exhibits a considerable variance across the six cores (from 0.07 to >0.5 a⁻¹). That these values are all significantly lower than the 1.25 a⁻¹ suggested by the kinetic experiments of VanCappellen and Qiu [1997b] may reflect fundamental differences between the in vitro and in situ environments.

[20] Since the presence of detrital material exerts an important kinetic influence [Dixit *et al.*, 2001; Rickert *et al.*, 2002; VanCappellen and Qiu, 1997b], we introduce a dependence of k_0^{opal} on the %detrital/%opal ratio. An empirical relationship is defined consistent with the fitted core-specific dissolution rates. The relationship is additionally constrained by assuming $k_0^{\text{opal}} = 1.25$ a⁻¹ in the absence of any detrital matter (i.e., $c^{\text{detrital}}/c^{\text{opal}} = 0.0$) [VanCappellen and Qiu, 1997b]. This gives the relationship (Figure 5)

$$k_0^{\text{opal}} = 0.05 + 0.055 \left(0.0164 \frac{c^{\text{detrital}}}{c^{\text{opal}}}\right)^{-0.75} \quad (15)$$

[21] The predictions of the complete model scheme (equations (14) and (15)) are contrasted with observational estimates [Rabouille *et al.*, 1997] in Table 1.

2.2. Water Column Opal Remineralization

[22] Simple exponential (with depth) functions were utilized to describe the remineralization of biogenic opal settling through the water column in early carbon cycle model studies [Maier-Reimer, 1993]. More recently, noting the importance of temperature in the control of dissolution rates, Gnanadesikan [1999] proposed a physically more realistic parameterization, with the dissolution rate of sinking siliceous material, r^{opal} (d⁻¹), described by

$$r^{\text{opal}} = 1.32 \times 10^{16} e^{\left(\frac{-11481}{T}\right)} \quad (16)$$

where T is the absolute temperature, and assuming a uniform settling rate of 50 m d⁻¹ throughout the water column. Although dissolution rate is also a function of the

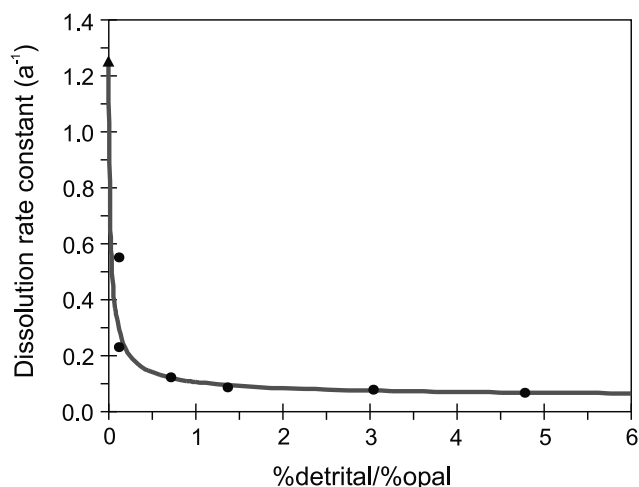


Figure 5. Dependence of k_0^{opal} on the ratio of detrital to opal sediment content. Model dissolution rates required to produce the estimated dissolution fluxes of *Rabouille et al.* [1997] are shown as filled circles, while the dissolution rate of pure opal under ambient conditions of 0°C and complete undersaturation [*VanCappellen and Qiu, 1997b*] is shown as a filled triangle. The empirical fit to this data is shown as a gray line.

degree of undersaturation, u^{opal} (equation (5)), it could be argued that since the ocean is everywhere far from saturation with respect to the solid phase, this additional dependence need not be taken into account. Indeed, a dominant temperature control upon dissolution appears to be consistent with early experimental observations [e.g., *Erez et al., 1982*]. However, this assumption requires that dissolution rate is not a strong function of u^{opal} in the vicinity of $u^{\text{opal}} = 1.0$. Evidence for nonlinear dissolution kinetics of opal [*Rickert et al., 2002; VanCappellen and Qiu, 1997b*] now suggests that such an assumption may not be safe. In the ocean interior, a combination of cold temperatures and relatively high ambient silicic acid concentrations can give rise to values of u^{opal} as low as ~ 0.8 in the deep Pacific. A temperature-only parameterization might then significantly overestimate opal dissolution in such locations.

[23] As an adjunct to the formulation of opal remineralization within the sediments, we present a new scheme for remineralization taking place within the ocean interior, one able to explicitly account for the influence of both ambient temperature and the concentration of silicic acid.

2.2.1. Model Formulation

[24] The parameterization for opal remineralization within the water column is a semi-empirical formulation based on observed thermodynamic behavior [*VanCappellen and Qiu, 1997a, 1997b*] and as such, shares a common basis with that for sedimentary diagenesis (section 2.1). Primary controls upon dissolution rate are assumed to be ambient temperature and the concentration of silicic acid. No account is taken of changes in surface reactivity during transit through the water column, such as might occur through a reduction in surface roughness, or the preferential removal of reactive

sites at surface defects [*Rickert et al., 2002; VanCappellen and Qiu, 1997b*].

[25] Recent work suggests that bacteria might mediate a fundamental transition in the dissolution rate of siliceous material [*Bidle and Azam, 1999*]. Remineralization of the opaline skeletons of live diatoms is suppressed by the presence of a protective organic coating. Removal of this coating (such as that occurs through bacterial action on lysed diatom cells) has been found to accelerate opal dissolution rates by an order of magnitude or more [*Bidle and Azam, 1999; Kamatani, 1982*]. For nonaggregating diatom detritus, the residence time in the mixed layer can be relatively long compared to the time taken for degradation of the organic coating [*Bidle and Azam, 1999*]. Degradation will then occur predominantly within the euphotic zone, with little further role for bacteria in controlling the remineralization of exported material. In contrast, under aggregating/rapid export events, setting rates may be sufficiently fast that degradation takes place during the passage of material through the ocean interior. In this situation, bacteria are likely to play a key role in determining the final remineralization profile. However, without any mechanistic treatment of aggregation (and associated setting rates) in the model, and in the absence of sufficient quantitative constraints on the details of the degradation process at present, we make the simplifying assumption that degradation of the protective coating occurs wholly within the euphotic zone. The implications of this are discussed subsequently.

[26] The dissolution rate of biogenic opal at depth d in water column, $F_{\text{dis}(d)}^{\text{opal}}$ (mol Si a^{-1}) is defined as

$$F_{\text{dis}(d)}^{\text{opal}} = \eta_{1(z)}^{\text{opal}} k_0^{\text{opal}} F_{\text{set}(d)}^{\text{opal}} \quad (17)$$

where k_0^{opal} is a base opal dissolution rate pertaining to ambient conditions of 0°C and complete undersaturation (with respect to the solid phase), $F_{\text{set}(d)}^{\text{opal}}$ is the settling flux of opal (mol Si a^{-1}), and $\eta_{1(z)}^{\text{opal}}$ is a normalized modifier of dissolution rate, as described previously (equation (8)).

[27] *Nelson et al.* [1976] reported a mean dissolution rate constant of small centric diatoms under different growth conditions equivalent to 0.134 d^{-1} at 20°C , while two acid-washed coastal species (also measured at 20°C) were observed to dissolve at a rate of 0.074 d^{-1} [*Kamatani, 1982*]. Dissolution rates can also be estimated in situ from observations of the rate of increase in $[\text{H}_4\text{SiO}_4]$ within the sediment trap headspace. In this way, *Brzezinski and Nelson* [1995] calculated the dissolution rate constant of trapped material as $0.07 \pm 0.03 \text{ d}^{-1}$ at $\sim 19^\circ\text{C}$, while *Blain et al.* [1999] estimated rates of 0.068, 0.085, 0.075, and 0.065 d^{-1} from a series of four different deployment depths. If conditions of complete undersaturation (i.e., $u^{\text{opal}} = 1.0$) are assumed, and dissolution rate constants temperature-corrected to $T = 0^\circ\text{C}$ (ambient temperatures being estimated from *Levitus et al.* [1994] where not reported) and using a Q_{10} value of 2.3 [*Kamatani, 1982*], a mean value for k_0^{opal} of 0.019 d^{-1} is obtained.

[28] Finally, to calculate the release rate of H_4SiO_4 within any given vertical interval of ocean, the settling rate of particulate material must be known. Analysis of sediment trap series suggests settling rates of opal material ranging from 32 to 200 m d^{-1} [*Blain et al., 1999; Honjo and*

Table 2. Biogenic Opal Flux Sediment Trap Data

Data Set	Location	Reference
1	17.5°N, 117.0°W	Noriki and Tsunogai [1986]
2	61.5°S, 150.5°E	Noriki and Tsunogai [1986]
3	31.7°N, 124.6°W	Noriki and Tsunogai [1986]
4	34°N, 21°W	Honjo and Manganini [1993]
5	13°N, 54°W	Honjo [1980] and Honjo et al. [1982]
6	50°N, 145°W	Takahashi [1986]

Manganini, 1993; Takahashi, 1986]. In the absence of any stricter observational constraint, a uniform sinking rate of 125 m d^{-1} is assumed [Pondaven et al., 1998].

2.2.2. Model Evaluation

[29] A number of studies have reported opal-settling fluxes measured simultaneously at multiple depths. Such data are vital for validating models of opal remineralization. However, there are a number of potential complications in the use of sediment trap observations in this way:

1. Since the ocean is undersaturated everywhere with respect to biogenic opal, material caught in sediment traps will continue to dissolve throughout the period of trap deployment. While more recent field campaigns have made use of traps filled with high-density brine solutions in order to help quantify in situ dissolution [e.g., Blain et al., 1999; Brzezinski and Nelson, 1995; Honjo and Manganini, 1993], early studies did not quantify such losses [e.g., Honjo, 1980; Noriki and Tsunogai, 1986; Takahashi, 1986]. Account must therefore be taken of the potential for older trap designs to underestimate settling fluxes.

2. Sinking fluxes may be modified by the random mesoscale eddy field through which the particles settle [Siegel et al., 1990], an effect that can distort the apparent flux profile. Even where flux measurements have been made by free-floating traps [e.g., Blain et al., 1999] there is still likely to be some residual hydrodynamic distortion.

3. Temporal variability in export production, such as associated with phytoplankton blooms, may cause problems for short-term trap deployments, with traps at different depths sampling different phases of the bloom succession.

4. In mesopelagic trap deployments, there is a danger that differences in the capture rates of radiolarians with depth may lead to some distortion of the apparent flux profiles [Blain et al., 1999].

[30] Filtering available data in light of the above considerations, six trap deployment data sets are selected for the validation exercise, listed in Table 2.

[31] For each data set, the opal remineralization model is used to predict the settling flux of opal that would be measured by the individual sediment traps. For this, a base dissolution rate constant (k_0^{opal}) of 0.019 d^{-1} is assumed, along with a uniform settling rate of 125 m d^{-1} [Pondaven et al., 1998]. Temperature and $[\text{H}_4\text{SiO}_4]$ profiles in the water column at trap locations are taken from Levitus et al. [1994] and Conkright et al. [1994], respectively. The mean residence time of opal in the traps is assumed to be equal to half the total trap collection time. During this period, opal is dissolved continuously at a rate dictated by ambient environmental conditions and is assumed “lost”,

since none of the selected sediment trap studies take account of in situ dissolution loss. Finally, for each data set, the magnitude of the opal export flux at 100 m depth is chosen so that the shallowest observed trap flux is reproduced. The model then simulates the flux that would be recorded by the deeper sediment traps.

[32] Simulated and observed trap fluxes are detailed in Table 3. It can be seen that the model can approximately simulate the change in flux with depth in a couple of the data sets (data sets 2 and 6). While the general trend exhibited by data set 3 (Table 3) is reproduced with an apparent maximum occurring at the 1250 m depth trap deployment, the magnitude of this feature is not well reproduced by the model. This mismatch can be corrected, however, by doubling the value of k_0^{opal} to 0.038, a value only slightly higher than the range that reported dissolution rates allow for. The remaining data sets are poorly simulated. For instance, dissolution in the relatively warm and highly under-saturated environment of the tropical Atlantic location of data set 5 is apparently seriously overestimated. This model-data mismatch might be explained if the unusually long trap deployment period of 98 days [Honjo, 1980; Honjo et al., 1982] results in geochemical conditions within the layer of accumulating material in the bottom of the trap to approach those of the abyssal sedimentary environment (particularly since this location lies within the Saharan dust plume [Duce et al., 1991]). The presence of detrital matter may thus have acted to suppress dissolution [Rickert et al., 2002; VanCappellen and Qiu, 1997a, 1997b], a factor accounted for in the scheme for sedimentary diagenesis (section 2.1.1), but not in the water column remineralization model applied in simulating the sediment trap data. Indeed, we find that it is possible to reproduce the observed profile by assuming a much lower value for k_0^{opal} (and in conjunction with a decrease in settling velocity).

[33] For comparison, the equivalent predictions made by Gnanadesikan’s [1999] parameterization (equation (16)) are shown alongside those of our model (Table 3). This model appears to consistently underestimate the trap observations in most of the data sets. An improved fit is possible if a more rapid settling rate is adopted, although it is beyond this particular scheme’s capability to fit either of the data set 3 or 5, regardless of the assumptions made regarding settling rate.

[34] Despite its deficiencies, the new parameterization presented here does enable certain features of the observed data to be captured that could not readily be achieved before, particularly the existence of flux maxima at intermediate depths. This apparent “increase” of opal flux with depth (exhibited by data sets 3, 4, and 5) probably results from the in situ dissolution loss as captured opal resides in a shallower trap being greater than the combined loss due to dissolution during transit to the depth of a deeper trap and residence in the deeper trap. Such a situation is facilitated by the existence of a relatively steep environmental gradient (primarily in u) between traps, and by a trap residence time long compared to the transit time between traps. Since the flux maxima occur relatively deep in the ocean (1250–3755 m), it is unlikely that this is an artifact of radiolaria “swimmers” [Blain et al., 1999]. There is also no evidence in co-recorded CaCO_3

Table 3. Modeled Versus Observed Opal Flux

Depth, m	Observed Opal Flux, $\mu\text{mol Si cm}^{-2} \text{ a}^{-1}$	Predicted ^a Flux, $\mu\text{mol cm}^{-2} \text{ a}^{-1}$	Predicted ^b Flux, $\mu\text{mol cm}^{-2} \text{ a}^{-1}$
<i>Data Set 1</i>			
470	3.5	(3.50) ^c	(3.50) ^c
690	3.0	3.74	3.54
1220	2.9	3.91	3.25
3340	3.0	3.64	2.16
3660	2.8	3.59	2.03
<i>Data Set 2</i>			
520	532.7	(532.7) ^c	(532.7) ^c
770	540.0	524.7	506.7
1200	473.0	513.0	469.8
2260	399.9	488.5	396.0
3110	484.6	466.7	346.9
<i>Data Set 3</i>			
500	1.2	(1.20) ^c	(1.20) ^c
720	1.7	1.33	1.21
1250	2.1	1.41	1.15
3380	1.9	1.35	0.79
<i>Data Set 4</i>			
1000	2.7	(2.70) ^c	(2.70) ^c
2000	3.4	2.41	2.03
4500	3.3	1.75	1.13
<i>Data Set 5</i>			
389	5.0	(5.00) ^c	(5.00) ^c
988	5.1	0.76	0.00
3755	5.4	0.00	0.00
5068	4.1	0.00	0.00
<i>Data Set 6</i>			
1000	61.2	(61.2) ^c	(61.2) ^c
3800	47.2	54.4	35.2

^a Present model (section 2.2).

^b Gnanadesikan [1999] parameterization.

^c In each case, the magnitude of the export flux at the base of the mixed layer in the model is chosen so that the shallowest sediment trap flux observation is reproduced.

and detrital fluxes to suggest that hydrodynamic effects are responsible. Such an artifact would not be expected to be observed in traps where in situ dissolution was accurately quantified.

[35] Accounting for spatial variability in the chemical (ambient silicic acid concentrations) and physical (temperature) environment is clearly not sufficient in itself. There must be additional processes (omitted from equation (17)), which need to be accounted for in order to successfully reproduce observed sediment trap fluxes. One possibility is that the assumption of an opal-settling rate, which is uniform both with depth and with location of trap deployment, is in error. For instance, there is good evidence that the settling velocity of particulate material increases with depth [Berelson, 2002; Honjo and Manganini, 1993; Siegel et al., 1990], while velocities tend to be higher at locations where export is dominated by aggregates and fecal pellets [Dixit et al., 2001]. A second possibility concerns the role of bacteria, which could drive a significant increase in dissolution rate as siliceous material settles down through the ocean interior and the initially present protective organic coating is degraded. Dissolution rates will subsequently

stabilize once the coating completely degrades or the material reaches the trap interior (invariably “poisoned” to prevent further (in situ) degradation of particulate organic material).

3. A Model for the Ocean Si Cycle

[36] Carbon cycle models incorporating the ocean-sediment Si cycle have already been developed [Archer et al., 2000b; Heinze and Crowley, 1997; Heinze et al., 1999]. However, these models operate on a relatively fine three-dimensional (3-D) ocean grid, and as a result can tend to be computationally quite expensive to run. It is therefore currently not entirely practical to generate large numbers of long (>100 ka) integrations with such models. To facilitate the characterization of the dynamics of relatively slow response components of the global carbon cycle (such as the oceanic inventory of silicic acid or the distribution of CaCO_3 on the sea floor) and enable extensive sensitivity analyses to be conducted, a much more efficient numerical representation of the system is highly advantageous. A model of the ocean-atmosphere-sediment carbon cycle developed for application on glacial-interglacial time scales is therefore employed here [Ridgwell, 2001]. In this model, the physical representation of ocean circulation is derived from an off-line version of the zonally averaged OGCM of Stocker and Wright [1996], providing a reasonable compromise between highly simplified and computationally efficient (but very poorly resolved spatially) “box” models [e.g., Peng and Broecker, 1993], and considerably more, computationally, expensive models based on 3-D OGCMs [e.g., Archer et al., 2000b; Heinze et al., 1999]. The model of Stocker and Wright also has the advantage that its utility in paleoceanographic biogeochemistry studies is well established [Marchal et al., 1998a, 1998b, 1999]. Access to multiple runs on glacial-interglacial timescales is additionally facilitated by degrading meridional and vertical resolution by a factor of ~ 2 [Ridgwell, 2001]. The resulting representation of the physical structure and circulation of the ocean is shown schematically in Figure 6.

[37] Ocean biogeochemistry is based on the cycling of three primary nutrients limiting to biological productivity; phosphate, silicic acid, and iron. This is similar to that used by Watson et al. [2000], with the main difference being that of the representation of remineralization of opal in the water column, for which the scheme described in section 2.2 is utilized.

[38] At the ocean surface, CO_2 and O_2 are exchanged with a “well-mixed” atmosphere. At the ocean floor, exchange takes place with the sediments - settling particulate material being added to the surface sediments, and dissolved species diffusing back into the overlying water. To predict burial rates of biogenic opal, the sedimentary opal diagenesis scheme described in section 2.1 is utilized. In order to capture the control of atmospheric $x\text{CO}_2$ exerted via the “rain ratio” mechanism [Archer and Maier-Reimer, 1994] that is at the heart of the Silica hypothesis [Harrison, 2000], it is necessary to account for the dissolution of CaCO_3 in the sediments, driven not only by the degree of undersaturation

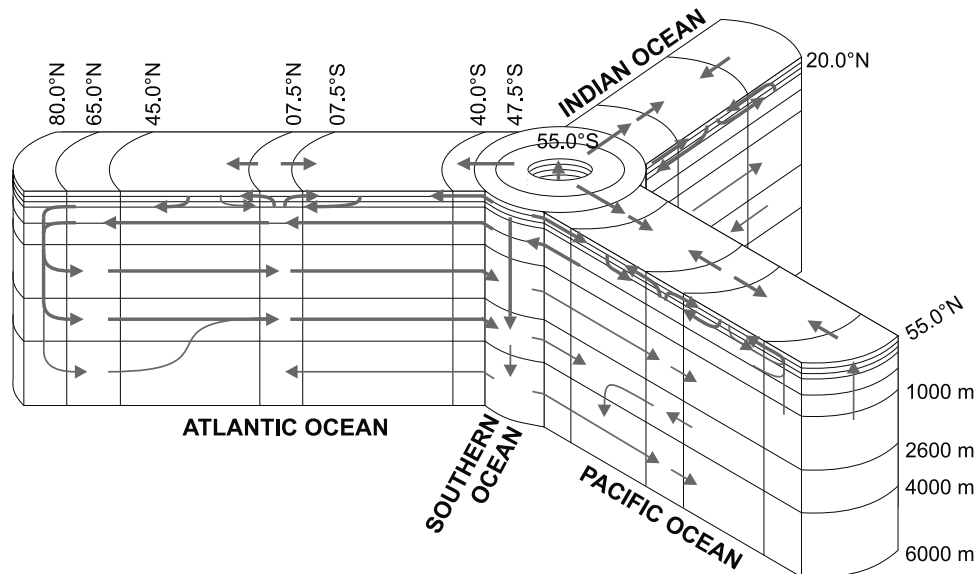


Figure 6. Ocean structure and schematic circulation field of the model.

(if any) of the overlying water (with respect to the solid phase) but also as a result of the respiration of organic carbon within the sediment pore water. To achieve this, we adopt the sedimentary CaCO_3 diagenesis model of Archer [1991], previously utilized to predict CaCO_3 preservation in the sediments within models addressing present-day sediment composition distributions [Archer, 1996], past (glacial-interglacial) changes in atmospheric $x\text{CO}_2$ [Archer and Maier-Reimer, 1994; Ridgwell, 2001; Watson *et al.*, 2000], and the future fate of anthropogenic CO_2 [Archer *et al.*, 1997].

[39] Further details of the representation of ocean circulation and of ocean-sediment biogeochemistry are given in the Appendix A, with the model fully described in its entirety by Ridgwell [2001].

3.1. Baseline Model Results

[40] A modern (pre-industrial) baseline simulation is generated by integrating the model for 500 ka following an initial 50 ka spin-up period. This is sufficiently long to bring even the slowest adjusting part of the system (^{13}C , with an adjustment time of ~ 100 ka) virtually into steady state. The supply rate of silicic acid to the open ocean (from net riverine influx, hydrothermal sources, and sea floor weathering - see Figure 1) was set at $5.1 \text{ Tmol Si a}^{-1}$, just slightly lower than estimated by Tréguer *et al.* [1995]. For aeolian Si input, we utilize the modern deposition field generated by the dust production-transport-deposition model of Mahowald *et al.* [1999], giving a total dust flux to the ocean of some $6.85 \times 10^{14} \text{ g a}^{-1}$. Assuming that the abundance of SiO_2 is 66 wt% (mean upper continental crustal abundance [Taylor and McLennan, 1985]), the SiO_2 input is $4.52 \times 10^{14} \text{ g SiO}_2 \text{ a}^{-1}$, or $7.54 \text{ Tmol Si a}^{-1}$. To achieve a value for aeolian silicic acid supply of $0.5 \text{ Tmol Si a}^{-1}$ [Tréguer *et al.*, 1995], a solubility of $\sim 6.6\%$ is required. This is in line with the experimental estimates [Wollast and Chou, 1985].

[41] The baseline model state is characterized by a mixing ratio of CO_2 in the atmosphere of 269 ppm. This is slightly lower than pre-industrial estimates of 278 ppm [Houghton *et al.*, 2001], possibly due to the simplistic partitioning of biological export between just two phytoplankton groups [Ridgwell, 2001; Watson *et al.*, 2000], poor representation of convective regimes at high latitudes, and/or lack of true seasonality in the model. Since the focus of this study is on the dynamical behavior of the ocean Si system over an extended time period, there is little to be gained from overtuning the model to achieve any particular steady state atmospheric $x\text{CO}_2$ value. Mean oceanic dissolved inorganic carbon (DIC), alkalinity (ALK), and H_4SiO_4 concentrations predicted by the model of 2234, 2370, and $74.5 \mu\text{mol kg}^{-1}$, respectively, are all in line with pre-industrial estimates [Tréguer *et al.*, 1995; Yamanaka and Tajika, 1996]. Total POC export out of the euphotic zone (100 m depth) is 8.8 Gt C a^{-1} , similar to current model estimates of $7.5\text{--}11.0 \text{ Gt C a}^{-1}$ [Archer *et al.*, 1998, 2000b; Heinze *et al.*, 1999; Six and Maier-Reimer, 1996; Yamanaka and Tajika, 1996]. Just over half of this (4.8 Gt C a^{-1}) is due to siliceous phytoplankton (diatoms) with the remainder being derived from nonsiliceous phytoplankton (including coccolithophorid) productivity. CaCO_3 export is 1.3 Gt C a^{-1} , giving a mean CaCO_3 :POC export rain ratio of 0.14, again consistent with current estimates, which lie in the range 0.08–0.22 [Archer *et al.*, 1998, 2000b; Heinze *et al.*, 1999; Yamanaka and Tajika, 1996].

[42] The model is moderately successful in reproducing some of the general features of the silicic acid concentration field in the ocean (Figure 7). However, it fails to reproduce observed ocean interior nutrient maxima in both the Pacific and Indian basins, while concentrations are too high closer to the surface (above ~ 500 m depth), possibly associated with a weak thermocline structure [Ridgwell, 2001]. The model also fails to fully resolve the deep H_4SiO_4 nutricline centered on the $75 \mu\text{mol kg}^{-1}$ contour. However, the

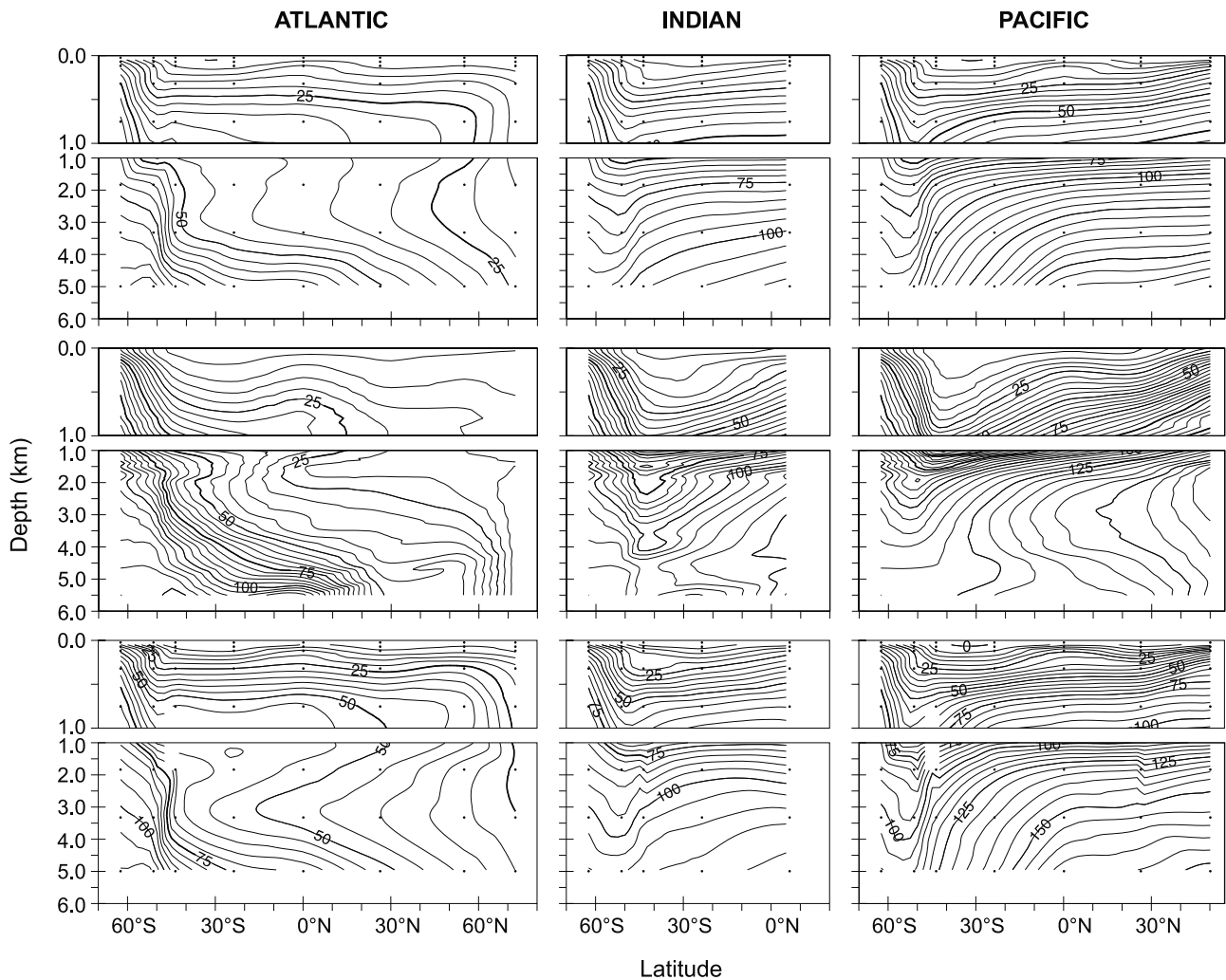


Figure 7. Ocean H_4SiO_4 field ($\mu\text{mol Si kg}^{-1}$); steady state results of the baseline model (top) and with the reconfigured Si cycle with lower opal settling rate and higher Si:C export ratios (bottom), compared with observations [Conkright *et al.*, 1994] (middle). The locations of cell centers in the model-generated results are shown as dots.

phosphate field (not shown), which is controlled by very different remineralization processes, exhibits similar deficiencies as that of H_4SiO_4 . This suggests that the low-resolution nature of the ocean structure and/or circulation may be predominantly to blame for such failures, rather than the biogeochemistry [Ridgwell, 2001]. It is also possible that this model-data misfit reflects the role of bacteria in degrading protective organic coatings, not accounted for in the present model. Since these coatings may only become completely degraded once the settling siliceous material has reached the ocean interior, dissolution rates (and thus the release of dissolved Si) would then be comparatively suppressed in the upper water column, thus explaining the unexpectedly low concentrations of H_4SiO_4 observed in the upper ~ 500 m.

[43] Global export of opal from the euphotic zone is $136.9 \text{ Tmol Si a}^{-1}$, somewhat lower than previous model-derived estimates of $170\text{--}275 \text{ Tmol Si a}^{-1}$ [Archer *et al.*, 2000b; Heinze *et al.*, 1999], but very close to mass balance estimates

of $\sim 120 \text{ Tmol Si a}^{-1}$ [Tréguer *et al.*, 1995]. Of this, $5.6 \text{ Tmol Si a}^{-1}$ accumulates in deep-sea sediments (balancing the dissolved Si input at steady state), giving an overall (i.e., water column + sedimentary) opal preservation efficiency of 4.4% with respect to export production. Assuming $\sim 50\%$ recycling efficiency within the euphotic zone [Nelson *et al.*, 1995], the mean global preservation efficiency of opal with respect to primary production is predicted to be 2.2%, consistent with previous estimates [Nelson *et al.*, 1995; Pondaven *et al.*, 2000; Tréguer *et al.*, 1995]. Model-predicted Si fluxes are shown schematically in Figure 1, and contrasted with the estimates of Tréguer *et al.* [1995].

[44] Although global opal export and burial fluxes predicted by the baseline model are consistent with the seminal analysis of the marine Si budget made by Tréguer *et al.*, there is obvious disagreement over how dissolution of biogenic opal is partitioned between water column and surface sediments. The baseline model predicts a total dissolution flux of $131.3 \text{ Tmol Si a}^{-1}$, partitioned with

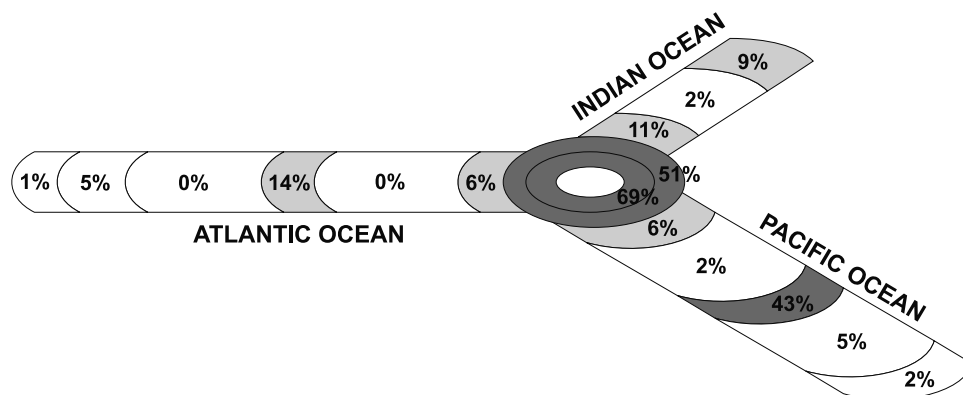


Figure 8. Mean wt% opal predicted in surface sediments lying deeper than 100 m in the ocean by the baseline model.

48.1 Tmol Si a⁻¹ occurring within the water column and 83.2 Tmol Si a⁻¹ in deep-sea sediments (Figure 1). In contrast, Tréguer et al. estimate losses due to water column processes to be greater by a factor of ~2, at 90.9 Tmol Si a⁻¹ (out of a total of 113.9 Tmol Si a⁻¹). In light of the rather disappointing performance of the remineralization model (section 2.2.2), an argument could be made for enhancing the degree of water column remineralization by reducing the assumed opal settling rate. To avoid distorting the concentration of H₄SiO₄ surface ocean and to retain other characteristics of the model pre-industrial carbon cycle (such as atmospheric xCO₂), the value of the (tunable) parameter controlling the Si:C export production ratio from siliceous phytoplankton (equation (27)) must also be adjusted. Reconfiguring the model with an opal settling rate reduced from 125 to 75 m d⁻¹, and increasing the Si:C ratio of siliceous phytoplankton export production by about 29% everywhere, a global dissolution rate of opal within the water column of 81.4 Tmol Si a⁻¹ is thereby obtained, which is comparable to the value obtained by Tréguer et al. (Figure 1). While total export in the model (165.9 Tmol Si a⁻¹) is now significantly greater than the 120 Tmol Si a⁻¹ estimated by Tréguer et al., a recent reassessment suggests that the data-based estimate (120 Tmol Si a⁻¹) must be revised upwards [DeMaster, 2002], bringing it more in line with this and previous model-based estimates [Archer et al., 2000b; Heinze et al., 1999]. The mean oceanic H₄SiO₄ concentration is now slightly higher than in the baseline model (82.6 compared to 74.5 μmol kg⁻¹). The model-predicted H₄SiO₄ field in the deep Pacific and Indian Oceans is now a better match to observations (Figure 7), although this is only achieved at the expense of a slightly poorer fit at shallower depths, adding further weight to an important role for a bacterial-mediated increase in opal dissolution rates with depth.

[45] The ~360% discrepancy between the global sediment dissolution flux predicted by the baseline model and the estimate of Tréguer et al. [1995] (Figure 1) is much less easy to resolve, and the situation is little improved (340%) with the alternative reconfigured Si cycle. Validation of the sedimentary diagenesis model (section 3.2) reveals no systematic deviation of model behavior from the observed data that is sufficient to account for the magnitude of the

mismatch. There are therefore no grounds to believe that the sedimentary opal diagenesis model can be substantially at fault. Another possibility is that the integrated Tréguer et al. global dissolution flux from deep-sea sediments is underestimated. For instance, while the baseline model predicts similar fluxes (~4 μmol Si cm⁻² a⁻¹) at the ocean-sediment interface underlying many oligotrophic regions, dissolution fluxes in the Antarctic region are higher by a factor of 2–3. In addition, Tréguer et al. implicitly discount any significant contribution made by sediments underlying low latitude upwelling zones, regions characterized by relatively high dissolution fluxes (10–60 μmol Si cm⁻² a⁻¹) in our model.

[46] The distribution of surface sediment opal content predicted in the baseline run is shown in Figure 8. Within the constraints dictated by a zonally averaged ocean circulation field, the global distribution appears generally reasonable compared to observations [Broecker and Peng, 1982; Heinze et al., 1999]. For instance, the prominent depositional environment in the Southern Ocean is correctly predicted. This is partly a result of high model opal export fluxes in this region, which arise due to a combination of siliceous phytoplankton dominated productivity and high opal:POC rain rates - itself a consequence of the model-parameterized (see Appendix A) effect of Fe availability on Si utilization efficiency by diatoms in this Fe-limited region. A second important factor is the relatively high degree of preservation of opal within the water column (up to twice as great as that in much of the rest of the ocean), driven by low temperatures and high concentrations of H₄SiO₄ [Ridgwell, 2001]. A subsidiary sink in the equatorial Pacific is also reproduced. However, little opal is present in Indian Ocean sediments contrary to observations, while opal contents in the equatorial Atlantic and north Pacific are slightly over-estimated. The distribution of sedimentary wt% opal is little affected by alternative (coupled) assumptions of lower opal settling rate and higher Si:C export ratios.

[47] More pertinent to the operation of the ocean Si cycle than the regional distribution of sediment opal content per se, are the respective burial fluxes. Detailed in Table 4 are the regional burial fluxes predicted by the baseline model and compared with the Tréguer et al. [1995] marine Si budget, and a recent re-assessment by DeMaster [2002]. It can be seen that burial rates both in (mainly oligotrophic)

Table 4. Estimates of Regional Deep Sea Sedimentary Si Sinks^a

	<i>Tréguer et al.</i> [1995]	<i>DeMaster</i> [2002]	This Study (Baseline Model)
Antarctic ^b	4.1–4.8	3.1	3.19
North Pacific ^c	0.3	0.3	0.23
Equatorial Pacific ^d	≪0.1	≪0.1	0.79
Equatorial Atlantic	0.81
Northern Indian Ocean	0.36
Opal-poor sediments ^e	<0.2	<0.2	0.26
Basins and seas ^f	0.7	0.7	(not resolved)
Total	5.1–6.0	4.1–4.3	5.62

^a Values are in Tmol Si a⁻¹.

^b 47.5°S to 70.0°S in the model (Figure 6).

^c 45.0°N to 55.0°N in the model (Figure 6).

^d 7.5°S to 7.5°N in the model (Figure 6).

^e Taken to be those characterized by <5 wt% opal in the model (Figure 8).

^f Specifically the Bering Sea and Sea of Okhotsk [*DeMaster*, 2002, 1981].

areas of low opal content sediments and in the North Pacific agree closely in all three studies. Our results are also highly similar to the recent (revised down) Antarctic budget [*DeMaster*, 2002]. However, there are disparities in the context of basin-scale sinks, which are not resolved in the model. There is also very substantial disagreement over the importance of low latitude upwelling regions, which we predict to be strong sinks, although problems of “nutrient trapping” [*Najjar et al.*, 1992] in the model may result in burial rates being somewhat overestimated, particularly for the equatorial Atlantic.

3.2. Validation of the Opal Diagenesis Model

[48] The sedimentary opal diagenesis model has been constructed semi-empirically, based on data derived from a single transect of sediment cores located in the Southern Ocean. It is therefore of obvious importance to carefully validate the model; ideally against data from geographically and biogeochemically different locations. Rather than focus on the detailed match to any one particular core or set of cores, because the diagenesis model is employed within a global framework, which resolves only mean regional (zonally averaged) behavior, it is arguably more appropriate to consider general trends of model behavior. A database of observations having direct equivalence with model output (and derived from cores located mainly in the tropical and subtropical Pacific and subtropical Atlantic) is assembled – detailed in Table 5 and presented graphically in Figure 9. Conditions in the regions where the cores are located deviate substantially from those of the Southern Ocean, often being characterized by much higher CaCO₃ sediment contents (especially in the Atlantic), lower opal rain rates, higher (Pacific) or lower (Atlantic) bottom-water silicic acid concentrations, and slightly warmer abyssal temperatures. Such data will thus provide a particularly robust test of the model.

[49] Global functional relationships between different variables (generated in the baseline run) exhibited by the opal diagenesis model are displayed in Figure 9. A number of observed trends are successfully reproduced, such as the variation of opal burial flux with rain flux (Figure 9a), opal content as a function of opal rain flux (Figure 9b), asymp-

totic sedimentary silicic acid concentrations as a function of sediment opal content (Figure 9e), and the relationship between asymptotic sedimentary silicic acid concentrations and opal rain rate (Figure 9d). Less well reproduced is the trend of dissolution flux as a function of opal content (Figure 9c), with the model unable to account for some of the very low dissolution fluxes observed in low- and mid-latitude regions. However, behavior critical to the global Si cycle, particularly the dependence of fractional burial on rain flux (Figure 9f), is still reasonably captured. Overall, considering that the opal diagenesis model was developed exclusively from Southern Ocean data, it is very encouraging that many aspects of its performance under very different oceanic and sedimentary conditions appear to be in such good agreement with observations.

4. Glacial-Interglacial Perturbation of Si Cycling

[50] Interest has recently been stimulated in the role that changes in the dissolved Si input to the ocean may have had in driving glacial-interglacial variability in atmospheric xCO₂ [*Harrison*, 2000; *Tréguer and Pondaven*, 2000]. Although a decrease in dust (as recorded at Vostok) precedes the increase in atmospheric xCO₂ at glacial termination [*Petit et al.*, 1999], there is an apparent lag of up to 8 ka between initial dust decline and initial xCO₂ rise [*Broecker and Henderson*, 1998]. For dust to drive the change in atmospheric xCO₂ at this time, this apparent lag must be accounted for. Since the residence time of H₄SiO₄ in the ocean is of similar order to the observed lag, an important role might be possible for changes in aeolian input of dissolved Si to the ocean. Based on this observation, *Harrison* [2000] proposed a “Silica Hypothesis”, whereby higher aeolian Si supply to the surface ocean during glacial times enhances diatom productivity at the expense of calcium carbonate shell-forming species, producing a second-order effect on xCO₂ through the “rain ratio hypothesis” [*Archer and Maier-Reimer*, 1994]. *Harrison* [2000] went further, and suggested that the entire deglacial increase in atmospheric xCO₂ might be explained by the decrease in dust supply to interglacial levels. Changes in the supply of Si from continental (silicate) rock weathering [*Tréguer and Pondaven*, 2000] or sea level driven fluctuations in opal accumulation on continental shelves [*Ridgwell*, 2001] might further enhance this effect.

[51] Although the delay between dust flux decline and atmospheric xCO₂ rise can be understood simply in terms of a nonlinear response of productivity in the Southern Ocean to changes in aeolian iron supply [*Ridgwell and Watson*, 2002; *Watson et al.*, 2000], it is also important to assess changes in Si input to the ocean as an alternative explanation. This assessment is made by integrating the carbon cycle model for approximately four glacial-interglacial cycles (400 ka), with an initial model spin-up of length 150 ka. A time history of dissolved Si supply to the ocean over the course of the last 400 ka is constructed by the transformation of a suitable proxy signal [*Ridgwell*, 2001]. The effect over time of this Si input perturbation on the ocean Si cycle and atmospheric xCO₂ is then analyzed.

Table 5. Details of Opal Diagenesis Model Sediment Core Validation Data

Core ID	Opal, wt%	Opal Rain Flux, $\mu\text{mol cm}^{-2} \text{a}^{-1}$	Opal Burial Flux, $\mu\text{mol cm}^{-2} \text{a}^{-1}$	Opal Dissolution Flux, $\mu\text{mol cm}^{-2} \text{a}^{-1}$	Preservation, %	$[\text{H}_4\text{SiO}_4]_{\text{asym}}$, $\mu\text{mol kg}^{-1}$	Reference
HAP	3	6	4.32 ^a	1.68 ^a	72		<i>Archer et al.</i> [1993]
NAP	0	4	0.04 ^a	3.96 ^a	1		<i>Archer et al.</i> [1993]
E	2	5					<i>Archer et al.</i> [1993]
MFZ	3	11	1.21 ^a	9.79 ^a	11		<i>Archer et al.</i> [1993]
ER	9	9					<i>Archer et al.</i> [1993]
NS	10	44	8.80 ^a	35.20 ^a	20		<i>Archer et al.</i> [1993]
MW	6	14	1.96 ^a	12.04 ^a	14		<i>Archer et al.</i> [1993]
G	3	5	0.20 ^a	4.80 ^a	4		<i>Archer et al.</i> [1993]
H	15	7	0.28 ^a	6.72 ^a	4		<i>Archer et al.</i> [1993]
M	11	12	0.48 ^a	11.52 ^a	4		<i>Archer et al.</i> [1993]
S	16	3	0.03 ^a	2.97 ^a	1		<i>Archer et al.</i> [1993]
C	13	11	1.10 ^a	10.90 ^a	10		<i>Archer et al.</i> [1993]
EP1	0	2					<i>Archer et al.</i> [1993]
PB	7	31					<i>Archer et al.</i> [1993]
T9	3.2			6.8			<i>Martin et al.</i> [1991]
T12	6.3			8.4			<i>Martin et al.</i> [1991]
T16	6.4			11.9			<i>Martin et al.</i> [1991]
T31	9.1			16.4			<i>Martin et al.</i> [1991]
T36	12.2			20.3			<i>Martin et al.</i> [1991]
T42	9.6			20.3			<i>Martin et al.</i> [1991]
T47	15.2			17.8			<i>Martin et al.</i> [1991]
T62	13.7			10.7			<i>Martin et al.</i> [1991]
T68	11.4			10.7			<i>Martin et al.</i> [1991]
T69	20.7			12.9			<i>Martin et al.</i> [1991]
T89	17.2			7.0			<i>Martin et al.</i> [1991]
T92	17.9			14.7			<i>Martin et al.</i> [1991]
04-12S				1.8		266	<i>McManus et al.</i> [1995]
10-12S				2.9		241	<i>McManus et al.</i> [1995]
34-05S				8.4		407	<i>McManus et al.</i> [1995]
39-05S				8.8		424	<i>McManus et al.</i> [1995]
27-05S	3.3			12.8		492	<i>McManus et al.</i> [1995]
19-02S				14.2		542	<i>McManus et al.</i> [1995]
23-02S	7.0			11.3		521	<i>McManus et al.</i> [1995]
48-00				14.6		537	<i>McManus et al.</i> [1995]
58-00				17.5		564	<i>McManus et al.</i> [1995]
77-02N				16.8		530	<i>McManus et al.</i> [1995]
82-02N	9.7			19.0		543	<i>McManus et al.</i> [1995]
113-04N	8.2			9.5		404	<i>McManus et al.</i> [1995]
104-05N	5.5			9.5		398	<i>McManus et al.</i> [1995]
108-05N				7.3		419	<i>McManus et al.</i> [1995]
132-09N	11.0			3.3		282	<i>McManus et al.</i> [1995]
135-09N				3.3		309	<i>McManus et al.</i> [1995]
Z-9				18.3		508	<i>McManus et al.</i> [1995]
X-5				17.2		474	<i>McManus et al.</i> [1995]
W-3				24.5		546	<i>McManus et al.</i> [1995]
PFC	7.8			11.3		461	<i>McManus et al.</i> [1995]
PFSC	9.6			5.1		415	<i>McManus et al.</i> [1995]
PFS	10.8			21.6		582	<i>McManus et al.</i> [1995]

^aCalculated from published opal rain rates and percentage opal preservation.

[52] Some care must be taken in the interpretation of the calculated atmospheric $x\text{CO}_2$ response. Concern has recently been raised regarding whether certain configurations of ocean carbon cycle model, particularly the so-called “box” models, might distort the response of atmospheric composition to certain perturbations [*Archer et al.*, 2000a; *Broecker et al.*, 1999]. To address this issue, two sensitivity indices have been independently developed for quantifying the relative control exerted by the high and low latitude ocean surface on atmospheric $x\text{CO}_2$ – the “Harvardton Bear Equilibrium Index” [*Broecker et al.*, 1999] and the “Abiotic Index” [*Archer et al.*, 2000a]. To verify that there is no a priori reason to suspect that the sensitivity of atmospheric $x\text{CO}_2$ to any Si perturbation might be biased

(at least in the context of the prescribed test environment), values for both of these indices are generated with the carbon cycle model used here. In both tests, score values are similar to those of carbon cycle models based on 3-D OGCMs [*Ridgwell*, 2001] (although this says nothing in itself regarding the absolute degree of realism or otherwise of the model response).

4.1. Testing the Silica Hypothesis

[53] To test the hypothesis that glacial-interglacial changes in aeolian Si supply could have exerted a strong control over atmospheric $x\text{CO}_2$, dust deposition to the surface ocean is varied. Dust production-transport-deposition models predict that the global dust flux to the ocean was a little over 3.3

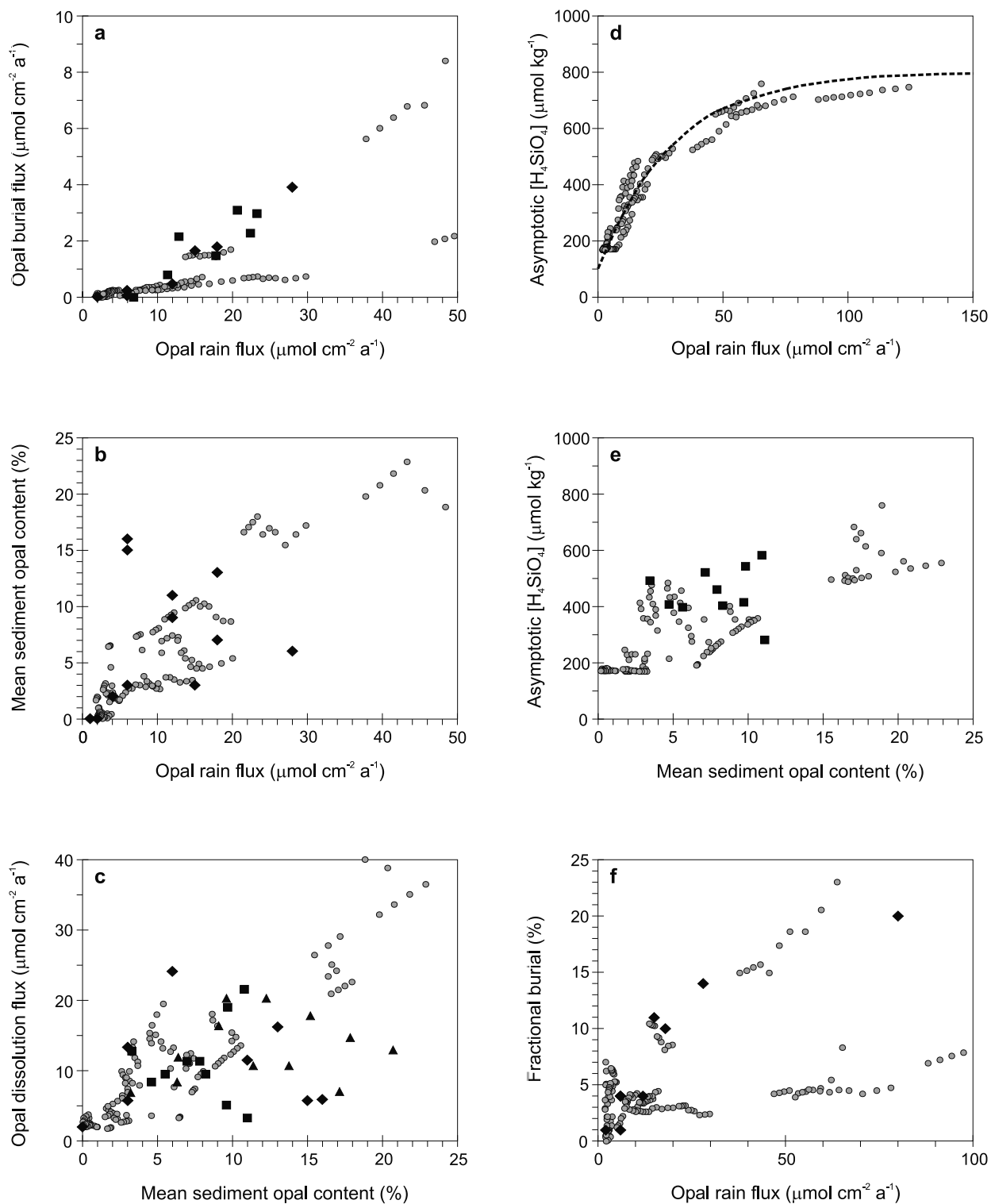


Figure 9. Functional relationships predicted by the opal diagenesis model at each sedimentary grid point (small open circles), but excluding sediments lying at depths shallower than 1000 m, contrasted with the validation data, indicated by larger filled symbols; squares - *McManus et al.* [1995], diamonds - *Archer et al.* [1993], triangles - *Martin et al.* [1991] (see Table 5). The thick dashed line in (d) indicates the estimated trend of *Archer et al.* [2000b]. The fragmentation of the overall trend into distinct segments of data points is an artifact of the discontinuous nature of biogeochemistry that results from the use of a relatively low-resolution representation of ocean circulation.

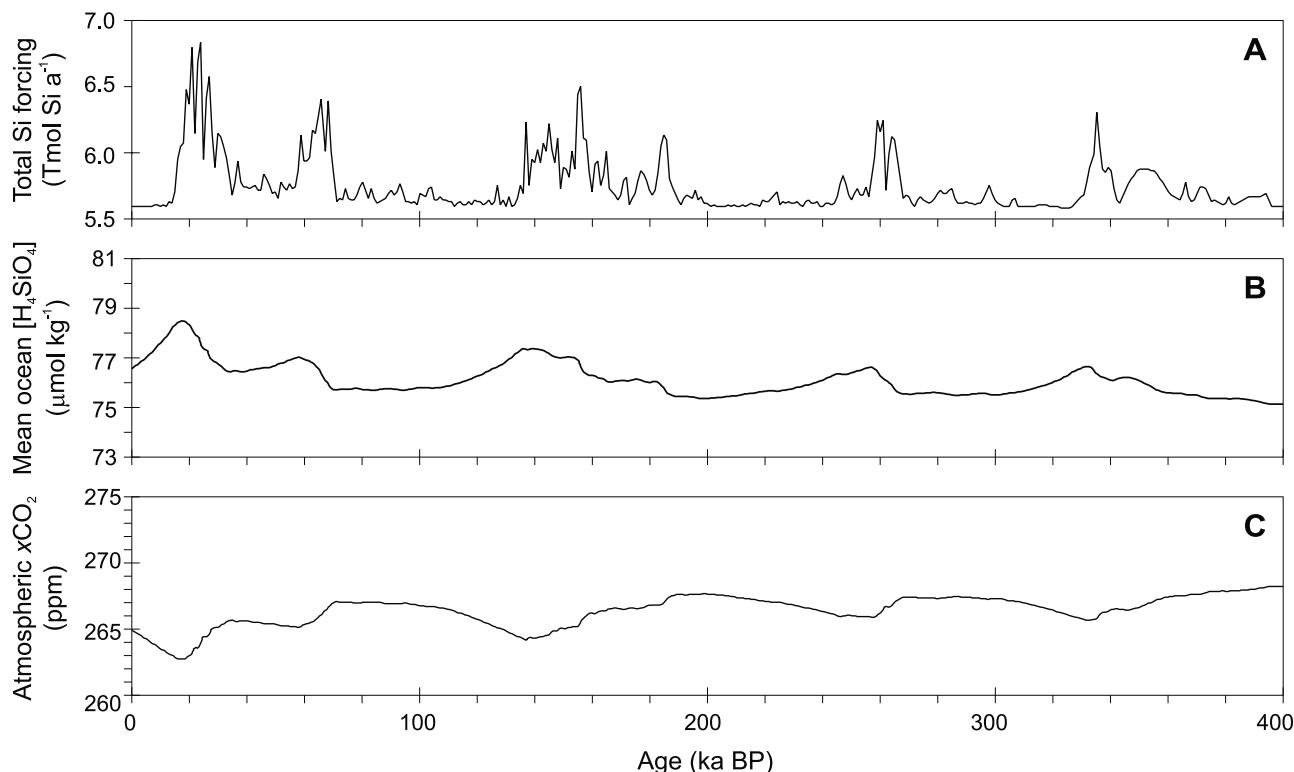


Figure 10. Response of the global carbon cycle to perturbation of aeolian Si supply. (a) Time history of dissolved Si supply to the ocean. (b) The oceanic Si inventory (as a mean silicic acid concentration). (c) Response of atmospheric $x\text{CO}_2$.

times higher during glacials than during interglacials [Mahowald *et al.*, 1999]. If present-day aeolian H_4SiO_4 supply is $0.5 \text{ Tmol Si a}^{-1}$ [Tréguer *et al.*, 1995], the glacial flux is then $1.67 \text{ Tmol Si a}^{-1}$. In order to reconstruct a record for the last 400 ka, the temporal variability of dust recorded in the Vostok core [Petit *et al.*, 1999] is used as a proxy for relative changes in flux [Watson *et al.*, 2000]. The resulting total dissolved Si supply signal is shown in Figure 10a. Aeolian iron supply, in contrast, is held constant for the purpose of this experiment.

[54] The response of the oceanic H_4SiO_4 inventory to the applied forcing is shown in Figure 10b. Despite a peak 20% perturbation in Si supply, the magnitude of variability induced in the H_4SiO_4 inventory is rather small (3%). Unlike the “Silica Hypothesis” [Harrison, 2000], the “biological” model employed in this study makes no assumption of invariant total global POC export (see Appendix A). Despite this, POC export is little affected ($<0.2\%$) by this perturbation in the baseline model. However, there is a 3.1% increase in global POC export flux derived from siliceous phytoplankton during glacial periods as compared to interglacials, which occurs at the expense of nonsiliceous phytoplankton productivity, reducing the global CaCO_3 :POC rain ratio by 3.6%. Atmospheric $x\text{CO}_2$ responds to this with a glacial-interglacial amplitude of less than ~ 4 ppm (Figure 10c), and with a total deglacial (19→0 ka BP) rise of little more than 2 ppm over the interval from 18 to 11 ka BP (during which ice cores show a relatively rapid rise of ~ 80 ppm [Petit *et al.*, 1999; Smith *et al.*, 1999]). The sensitivity of atmospheric $x\text{CO}_2$ to the Si perturbation is essentially the same under an

ocean Si cycle reconfigured to exhibit much greater dissolution of biogenic opal within the water column.

4.2. Introducing the “Opal Extraction Mechanism”

[55] We propose an additional mechanism by which the input of Si to the ocean might have been significantly altered on glacial-interglacial time scales. Recognizing that an analogue to the phosphate extraction model [Broecker, 1982; Broecker and Peng, 1982] can be found in the nutrient silicic acid, we suggest that the global accumulation rate of biogenic opal deposited on continental shelves may have varied substantially in response to changes in sea level. Considering that the burial of biogenic opal in neritic sediments is estimated to be equivalent to $\sim 20\%$ of the entire deep-sea sediment sink of H_4SiO_4 ($5.9 \text{ Tmol Si a}^{-1}$) [Tréguer *et al.*, 1995], operation of this mechanism represents a potentially significant perturbation of the oceanic Si cycle.

[56] A simple neritic opal accumulation model is constructed, parameterized after the (nonreefal component) CaCO_3 accumulation model of Munhoven and Francois [1996]. Rates of opal accumulation per unit shelf area are chosen to give a mean global accumulation rate over the late Holocene of $1.2 \text{ Tmol Si a}^{-1}$ [Tréguer *et al.*, 1995]. Since little is known regarding erosion rates of previously deposited opaline material, we depart from the CaCO_3 model of Munhoven and Francois [1996] by omitting any erosion term. The opal accumulation model is forced with a time-varying change in sea level reconstructed for the last 400 ka, taking the SPECMAP stacked $\delta^{18}\text{O}$ record [Imbrie *et al.*, 1984] as a signal template, and assuming that sea level at

the last glacial maximum was 117 m lower than at present [Fairbanks, 1989; Walker and Opdyke, 1995].

[57] This “opal extraction model” predicts a variable (as a function of sea level) neritic sink between 0.36 and 1.21 Tmol Si a⁻¹. Again, despite the applied forcing representing an apparently substantive perturbation of Si supply, the response of the oceanic H₄SiO₄ inventory and atmospheric xCO₂ is highly damped (not shown), with a deglacial increase of only ~2 ppm [Ridgwell, 2001].

5. Discussion

5.1. Atmospheric xCO₂ Sensitivity to Changes in Si Input

[58] As described in Appendix A, the ratio of CaCO₃ to POC exported out of the euphotic zone in the model is controlled by the partitioning of nutrient utilization between the two distinct phytoplankton groups [Ridgwell, 2001; Watson *et al.*, 2000] – siliceous phytoplankton (which are assumed responsible for the export of POC and opal) and nonsiliceous phytoplankton (which are assumed responsible for the export of POC and CaCO₃). In the absence of any nutrient limitation, siliceous phytoplankton dominate nutrient uptake and export. Supply of H₄SiO₄ therefore acts as a crude switch in the model. If the supply of H₄SiO₄ is plentiful, export of biogenic matter is dominated by siliceous phytoplankton, resulting in a low value for the CaCO₃:POC rain ratio. If H₄SiO₄ is limiting, however, nutrient uptake (and export) by siliceous phytoplankton is restricted, and the availability of other nutrients (PO₄ and Fe) for utilization by nonsiliceous phytoplankton will be greater. In this case, the CaCO₃:POC rain ratio will be relatively high. By increasing the supply of H₄SiO₄ to the euphotic zone, the rain ratio is shifted between these two extremes, and CaCO₃:POC ratio is reduced.

[59] In ocean sediments, the dissolution rate of CaCO₃ is a function of the degree of undersaturation of the aqueous pore water environment with respect to the solid (calcitic) phase [Hales and Emerson, 1997; Keir, 1980]. However, pore water carbonate chemistry is determined not only by the chemistry of the overlying waters, but also by the release of CO₂ through the respiration of organic matter (delivered along with CaCO₃) also present in the sediments [Archer, 1991, 1996; Emerson and Bender, 1981]. The fractional preservation of CaCO₃ in the sediments will therefore be perturbed by any change in the CaCO₃:POC rain ratio reaching the ocean floor. This, in turn, will upset the balance between the supply of carbon and alkalinity to the ocean, and CaCO₃ burial in (deep-sea) sediments, altering ocean chemistry and with it, atmospheric xCO₂. The sensitivity of atmospheric xCO₂ to changes in the global mean rain ratio in the model is about 1.6 ppm per percent change in CaCO₃:POC. A 40% decrease in rain ratio is therefore sufficient to drive a 68 ppm decrease in atmospheric xCO₂. This is comparable to the sensitivity found with a very different representation of ocean circulation and productivity (although with an almost identical representation of sedimentary CaCO₃ diagenesis) [Archer and Maier-Reimer, 1994].

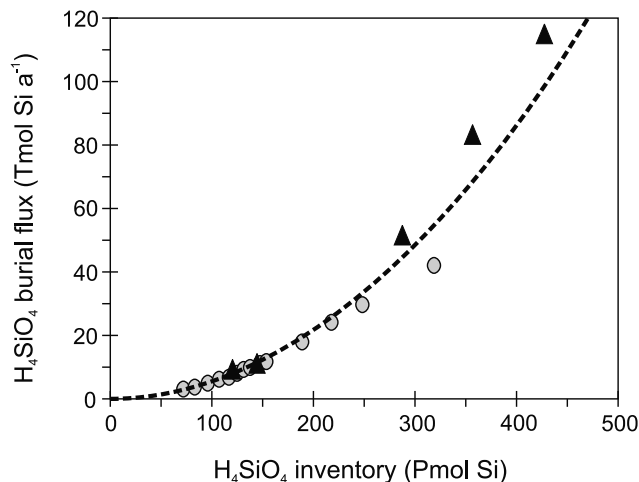


Figure 11. Response of global opal burial rate to changes in silicic acid inventory, predicted by Archer *et al.* [2000b] (filled triangles) and this study (circles). The best fit power law (power = 2.0) to the combined data is also shown (dashed line). For reference, the present-day ocean is characterized by an H₄SiO₄ inventory of around 100 Pmol Si [Tréguer *et al.*, 1995].

[60] The results of the ocean carbon cycle model presented here suggest that the response of the system to perturbation of dissolved Si supply to the ocean will be highly damped (see Figure 10). In contrast, an important role for reduction in Si supply in driving the deglacial rise in atmospheric xCO₂ was concluded in previous assessments made of the “Silica hypothesis” [Harrison, 2000; Tréguer and Pondaven, 2000]. A number of factors contribute to this discrepancy.

[61] Taking the slightly more realistic of the two assumptions made regarding ecosystem function, Harrison [2000] estimated that a 57% increase in opal export driven by an enhancement of aeolian Si supply (from 0.5 to 3.7 Tmol Si a⁻¹) would be sufficient to suppress the CaCO₃:POC rain ratio by 40%, and thus achieve a glacial atmospheric xCO₂ value [Archer and Maier-Reimer, 1994]. This is similar to the sensitivity found by Tréguer and Pondaven [2000] using an ocean biogeochemical model [Tyrell, 1999]. On a global basis, upwelling and mixing dominate the supply of new (i.e., not recycled) H₄SiO₄ to the euphotic zone [Tréguer *et al.*, 1995] (Figure 1). Therefore, for the Silica hypothesis to realize its full potential, changes in Si input must be capable of driving an ~50% increase in the oceanic H₄SiO₄ inventory.

[62] In assessing the Silica hypothesis, it is crucial to recognize that the global Si cycle is far from linear. Archer *et al.* [2000b] reported that the global opal burial rate scaled with the second power of ocean H₄SiO₄ inventory in a 3-D OGCM-based carbon cycle model. This is further investigated by carrying out a sensitivity analysis with the present model. Following a 50 ka spin-up under baseline (modern ocean) boundary conditions, a step-wise change in the total dissolved Si input to the ocean is imposed, and the system allowed to adjust for a further 50 ka (thus achieving ~95% of true steady state). The results of this analysis are shown in Figure 11. There is a clear nonlinear response of

burial flux with H_4SiO_4 inventory, with an approximately parabolic relationship, consistent with Archer et al. Since loss of opal through burial must equal the supply rate to the ocean of dissolved Si at steady state, the consequence of this nonlinearity is that it becomes disproportionately difficult to enhance the oceanic H_4SiO_4 inventory through an increase in Si supply [Archer et al., 2000b]. Opal export (and the CaCO_3 :POC rain ratio) will therefore be much less sensitive to changes in Si input to the ocean than predicted previously with the implicit assumption of a linear relationship between H_4SiO_4 inventory and Si supply. Taking this nonlinearity into account, the change in rain ratio corresponding to an increase in aeolian Si supply of $3.2 \text{ Tmol Si a}^{-1}$ would only shift ecosystem composition sufficiently to drive a decrease in rain ratio of $\sim 18\text{--}24\%$ on the basis of the models of Harrison [2000] and Tréguer and Pondaven [2000]. Our surface ocean productivity model predicts a similar (20%) decrease in rain ratio in response to the same (steady state) increase in Si input, sufficient to lower atmospheric $x\text{CO}_2$ by 34 ppm.

[63] Secondly, the 7.4-fold glacial enhancement in aeolian silicate delivery assumed by Harrison [2000] and Tréguer and Pondaven [2000] is more than double the prediction of a dust production-transport-deposition model (3.3 times) that we adopt [Mahowald et al., 1999]. Taking this lower estimate, the change in rain ratio would be further reduced to $\sim 10\%$, with the silica hypothesis now only accounting for a ~ 14 ppm change.

[64] Finally, it is important that account is taken of the time-varying nature of the system forcing. Some of the more prominent features exhibited by records of dust supply (such as associated with deglacial transitions and glacial maxima) are characterized by time scales of order 10 ka or less [DeMenocal et al., 1993; Petit et al., 1999; Rea, 1990; Tiedemann et al., 1994]. This is shorter than the oceanic residence time of H_4SiO_4 in the ocean, which has a value of about 16 ka in our model, consistent with estimates of 10–20 ka derived from previous modeling [Archer et al., 2000b] and mass balance [Tréguer et al., 1995] considerations. The response of the oceanic H_4SiO_4 inventory to a time-varying perturbation in supply rate will therefore be damped. Furthermore, it is not the dynamical response of the ocean Si system that is of ultimate interest, per se, but atmospheric trace gas composition. Since changes in sedimentary CaCO_3 burial controls atmospheric $x\text{CO}_2$ in the silica hypothesis, the additional response of the ocean-sediment CaCO_3 system to perturbation of the CaCO_3 :POC rain ratio must be taken into account. In our model this is ~ 9 ka, consistent with Archer et al. [1997]. The e -folding time of atmospheric $x\text{CO}_2$ with respect to changes in Si supply will therefore be slower than that of the oceanic Si inventory alone. We find that atmospheric $x\text{CO}_2$ in fact responds with an e -folding time of about 23 ka. Ocean-sediment interactions thus act as an efficient low-pass filter on a time-varying input of Si to the ocean.

[65] The net consequence of these different factors is that decreasing aeolian silicate deposition rates are unable to account for any significant proportion of the rapid deglacial increase observed in atmospheric $x\text{CO}_2$. Similar arguments can be applied to glacial-interglacial variability in riverine

H_4SiO_4 supply from weathering, and to our “opal extraction mechanism.” Furthermore, the fact that the response time of the oceanic Si inventory (and thus of atmospheric $x\text{CO}_2$) depends on the ratio of inventory to total burial rate, suggests that the baseline model may represent something of an upper limit of sensitivity. Enhancing the importance of opal dissolution within the water column will result in an increased Si inventory, while lower glacial sea levels will result in a restricted (neritic) sedimentary sink – both these factors will increase the inventory to burial ratio and thus tend to drive an increased damping of system response to perturbation.

[66] Although the long adjustment time of the global carbon cycle results in a very muted atmospheric $x\text{CO}_2$ response associated with the relatively rapid deglacial transitions, this will not necessarily be the case with regard to the more gradual descent of the Earth system into its glacial state, which takes place on a time scale of 50–100 ka. Combined, changes in dust deposition and neritic opal accumulation rates can account for up to 10 ppm of the decrease in atmospheric $x\text{CO}_2$ between each interglacial and subsequent glacial maximum. If a substantial glacial increase (50%) in the riverine supply of dissolved Si to the ocean arising from terrestrial weathering were also to be hypothesized, it is possible that an increasing oceanic inventory of H_4SiO_4 could perhaps drive as much as 20 ppm of the declining trend evident in each climatic cycle [Petit et al., 1999]. However, it should be noted that recent studies find little evidence for any significant glacial-interglacial change in the supply of dissolved Si from continental erosion [Jones et al., 2002].

5.2. Is the Present-Day Marine Si Cycle In or Out of Balance?

[67] Budgets constructed for the marine Si cycle have postulated that the system is close to steady state at present [DeMaster, 2002; Tréguer et al., 1995], with losses (opal burial) approximately equal to inputs (dissolved Si). If significant glacial-interglacial changes in the input of dissolved Si to the ocean have occurred, whether driven by variability in the flux of aeolian material to the ocean surface or through changes in the shelf area available for opal accumulation in neritic sediments (our “opal extraction mechanism”), the relatively long residence time of Si in the world ocean (~ 16 ka) raises the possibility that the present-day marine Si budget may be significantly out of balance. This would not make this biogeochemical cycle unique – for instance, it is suspected that the modern ocean nitrogen cycle is far from steady state, with nitrogen losses from the ocean through denitrification (particularly on continental shelves) exceeding the combined input from rivers, atmosphere, and nitrogen fixation in the surface ocean [Berger and Vincent, 1986; Codispoti, 1995; McElroy, 1983].

[68] A recent re-analysis of the marine Si budget [DeMaster, 2002] suggests a considerably greater role for neritic accumulation (at the expense of reduced accumulation in the deep-sea) than previous studies have identified [Tréguer et al., 1995]. On the face of it, this would appear to greatly enhance the potential importance of the “opal extraction

mechanism". However, there are difficulties in reconciling the revised *DeMaster* [2002] budget with the operation of this mechanism. The reasoning is as follows. We first assume that there is no change in riverine [Jones *et al.*, 2002] or hydrothermal and (cold) basaltic weathering fluxes (combined input to open and coastal ocean = 6.2 Tmol Si a⁻¹ [Tréguer *et al.*, 1995]). Making the same assumptions regarding aeolian Si input as earlier (section 4.1), suggests an aeolian contribution averaged over the past 400 ka of 0.65 Tmol Si a⁻¹ (interglacial = 0.5 Tmol Si a⁻¹, peak glacial = 1.2 Tmol Si a⁻¹). If there is to be no long term ($\gg 100$ ka) trend over the late Quaternary, the total (neritic + benthic) biogenic opal sedimentary sink averaged over a glacial-interglacial cycle must be equal to the total 6.85 Tmol Si a⁻¹ input. Since this falls near the bottom of the range of values (6.5–7.4 Tmol Si a⁻¹) that *DeMaster* [2002] estimates for the present-day total removal rate, peak glacial removal rates cannot be significantly lower, otherwise the long-term average sink would be out-of-balance with the input. This does not appear to be compatible with the very significant changes in shelf (and thus available depositional) area that occurred, particularly since weathering of neritic deposits of siliceous material on shelves exposed at times of low sea level stand would push the long-term balance even further into surplus.

[69] One possibility is that revised *DeMaster* [2002] marine Si budget significantly underestimates the magnitude of the removal rate in the deep-sea, with rates actually being more like the ~ 6 Tmol Si a⁻¹ predicted by our model and in the analysis by Tréguer *et al.* [1995]. In this case, the marine Si cycle would be out of balance at present, with a significant excess of burial compared to input. Alternatively, the present-day deep-sea sink might be as low as ~ 4 Tmol Si a⁻¹ as suggested by *DeMaster* [2002], but would have varied with time and been substantially higher during glacial periods. This could arise if the fractional preservation of opal deposited to deep-sea sediments was enhanced by a greater glacial (aeolian) detrital flux, which is consistent with the operation of our diagenetic model (equations (11) and (12)). In this case, the system could be out of balance at present but in the opposite sense, with an excess of Si input over output. Until the constraints on the marine Si budget are further improved, particularly with respect to the relative role of neritic versus benthic accumulation, it would appear that even the sign of any imbalance of the present-day system is uncertain, let alone its magnitude.

6. Conclusions

[70] We have developed a model of the dissolution of biogenic opal in deep-sea sediments, based on both theoretical and data considerations. Despite taking its empirical basis exclusively from Southern Ocean sediment core data, a validation exercise demonstrates that model predictions under very different biogeochemical environments are in good agreement with observations.

[71] We have also developed a new description for the remineralization of opal within the water column (and which shares a common mechanistic basis with the sedimentary diagenesis model). Although it takes into account

ambient conditions not only of temperature, but also uniquely, the degree of undersaturation with respect to the solid phase, when used to simulate observed sediment trap data, the improvement over previous schemes is only minor. In validating the water column remineralization model at the level of the raw data (integrated sediment trap flux), we demonstrate that additional factors clearly need to be taken into account. As likely candidates in this, we identify: (1) the dependence of the sinking velocity of siliceous material on both the surface ocean environment and with depth in the water column, and (2) the role of bacteria in degrading protective organic coatings. However, while the distribution of H₄SiO₄ in the ocean is relatively sensitive to how the dissolution of biogenic opal is distributed between the water column and the surface sediments, the overall response of the Si inventory to perturbation is not.

[72] Descriptions of opal sedimentary diagenesis and water column remineralization are incorporated into a model of the global ocean carbon cycle. The numerical efficiency of this model enables integration on glacial-interglacial time scales and extensive sensitivity analyses to be performed. Despite the relative simplicity of the zonally averaged representation of ocean circulation employed, many of the important features of the ocean-sediment Si system are captured, specifically; the global distribution of opal-rich sediments, and the net burial rate of opal required to balance independent estimates of the dissolved Si input to the open ocean. The sensitivities of the oceanic Si inventory to perturbation of Si input, and atmospheric xCO₂ to changes in the global CaCO₃:POC rain ratio are also found to be almost identical to those exhibited by much higher resolution 3-D models [(Archer *et al.* [2000b] and Archer and Maier-Reimer [1994], respectively)].

[73] The results of our model do not support explanations for the deglacial rise in the atmospheric mixing ratio of CO₂ as a consequence of decreasing Si supply to the ocean. A new hypothesis involving glacial-interglacial variability in neritic opal storage presented in this article is similarly ineffective in accounting for rapid atmospheric xCO₂ changes. However, in the context of the much slower climatic change as (following each interglacial) the Earth descends into its glacial state, increased Si supply to the ocean may be more important, and could potentially account for up to a fifth of the observed total atmospheric xCO₂ decrease.

[74] The adjustment time of the ocean silicic acid inventory is ~ 16 ka, while the calcite lysocline relaxes with an *e*-folding time of ~ 9 ka. The Si and CaCO₃ cycles interact to produce a response of atmospheric xCO₂ with respect to perturbations of Si supply characterized by an *e*-folding time of ~ 23 ka, significantly longer than that of either the ocean-sediments Si or CaCO₃ cycles alone. Deep-sea sediments, in co-determining the ratio of the oceanic inventory to loss (burial) rate of biogenic material, exert a fundamental control on some of the slower response components of ocean carbon cycle. This highlights the importance of using coupled ocean-sediment models in the assessment of climatic change on glacial-interglacial time scales. However, results from traditional methodologies whereby paired time slices made at steady state on either side of the last deglacial

transition (an interval shorter than the 23 ka response of the global carbon cycle identified here) are contrasted, must be treated with caution.

Appendix A

A1. Overview

[75] The atmosphere-ocean-sediment carbon cycle model of *Ridgwell* [2001] is employed here. This is based on a zonally averaged representation of ocean circulation, with ocean-atmosphere biogeochemistry similar to that utilized in studies of the effects of glacial-interglacial [*Watson et al.*, 2000] and anthropogenic [*Ridgwell et al.*, 2002] changes in aeolian iron supply to the ocean. Tracers advected in the ocean component include total DIC, dissolved oxygen (O_2), ALK, temperature, and salinity. Of these, CO_2 and O_2 are exchanged with a “well-mixed” atmosphere across the air-sea interface. The stable isotopes of carbon (^{12}C and ^{13}C) are treated separately, with all major fractionation processes between them taken into account. Three nutrients potentially limiting to biological activity in the ocean are considered; phosphate (PO_4), silicic acid (H_4SiO_4), and total dissolved iron (Fe). Nutrients, together with DIC and ALK, are taken out of solution in the sunlit surface ocean layer (“euphotic zone”) through biological action, and exported in particulate form (as POM, $CaCO_3$, and opal) to deeper layers. As it settles through the water column, such material is subject to remineralization processes, resulting in the release of dissolved constituent species to the ocean. Significant export of nutrients and carbon in the form of dissolved organic matter is not considered. Biogenic and detrital material reaching the ocean floor may undergo diagenetic alteration (representing a further release of dissolved species to the ocean) and/or (semi-) permanent burial. To accomplish this, the ocean is everywhere underlain by a series of discrete sediment modules handling ocean-sediment interactions, in which the preservation of biogenic $CaCO_3$ and opal reaching the sediment surface is explicitly predicted. Loss of material through burial in the sediments is balanced over the long-term by prescribed inputs to the system representing supply to the ocean from continental weathering and geothermal processes (in the case of DIC, ALK, and H_4SiO_4) together with aeolian input at the surface (Fe and H_4SiO_4).

[76] Complete descriptions of model configuration and validation against present-day observations have been described by *Ridgwell* [2001]. Details of the model pertinent to the perturbation response of the ocean Si inventory and atmospheric xCO_2 are given in the following sections.

A2. “Physical” Ocean Environment

[77] The representation of ocean circulation used is derived from an off-line version of the zonally averaged OGCM of *Stocker and Wright* [1996]. To increase computational efficiency (thus allowing improved access to glacial-interglacial time scales), meridional and vertical resolution is degraded. A structure of meta-cells is defined in the ocean, each of which encompasses multiple cells of the original model. By integrating fluxes across each of the meta-cell boundaries (and accounting for both net advection and exchange (mixing) components of the original circulation

field), a simplified ocean representation is obtained [*Michel et al.*, 1995]. The “child” structure utilized here is that adapted from the work of *Ridgwell* [2001], comprising 16 grid points in the horizontal with eight in the vertical (the corresponding lower boundaries in the “parent” OGCM [*Stocker and Wright*, 1996] begin located at depths of 50, 100, 150, 500, 1000, 2500, 3500, and 4000 m). Ocean structure and circulation are shown schematically in Figure 6. In addition to advection, transport of tracers also occurs diffusively in the ocean. Vertical diffusivity is varied down through the water column following the description given by *Weaver and Sarachik* [1991]. A coefficient of $1 \times 10^4 \text{ m}^2 \text{ s}^{-1}$ is assumed for horizontal diffusivity, consistent with values used in other intermediate and low-resolution ocean models [*Hovine and Fichefet*, 1994; *Rich et al.*, 1999].

A2.1. Seasonality

[78] Ocean circulation in the version of the Bern 2-D model used to derive the “child” model is in the form of an annual mean [*Marchal et al.*, 1998a]. To improve the representation of seasonal high latitude processes, a crude pseudo-seasonality in sea ice cover and convection is imposed [*Ridgwell*, 2001], taking its timing from monthly insolation [*Bacastow and Maier-Reimer*, 1990; *Holtslag and VanUlden*, 1983].

A2.2. Sea Ice

[79] Fractional sea ice coverage is varied at a monthly time step according to relative insolation levels. Sea ice extent is assumed to be in simple anti-phase with insolation, giving

$$A_{f(t)}^{\text{ice}} = A_{f,\text{min}}^{\text{ice}} \left(A_{f,\text{max}}^{\text{ice}} - A_{f,\text{min}}^{\text{ice}} \right) \frac{I_{\text{max}} - I(t)}{I_{\text{max}} - I_{\text{min}}} \quad (\text{A1})$$

where for each grid point, $A_{f(t)}^{\text{ice}}$ is the fractional sea ice-cover for month t , $A_{f,\text{max}}^{\text{ice}}$ and $A_{f,\text{min}}^{\text{ice}}$ are the observed maximum and minimum fractional coverages, respectively, with insolation (I) variables, similarly designated. Reconstructed sea ice limits are derived from *CLIMAP* [1984].

A2.3. Convection

[80] Because of the low resolution and annually averaged nature of the representation of ocean circulation, the effects of high latitude convective processes must necessarily be highly parameterized. We identify three different aspects of convection of particular importance to the ocean Si cycle:

1. Seasonal deepening of the mixed layer – During winter, surface nutrients are replenished through the entrainment of relatively nutrient-rich waters from below. This cycle is approximated by allowing a deepening of the surface ocean mixed layer when monthly insolation falls below a predetermined threshold (set to give a plausible 4–6 month-long “winter” season south of $\sim 55^\circ S$). Biological export is assumed negligible at this time. If the water column becomes convectively unstable during this period, convective adjustments are made by pair-wise homogenization of cells [*Wright and Stocker*, 1992]. To prevent excessive deep ventilation, mixing depth is restricted according to the mean maximum observed mixed-layer depth [*Levitus and Boyer*, 1994; *Levitus et al.*, 1994].

2. Formation of deep cold water masses – Deep ocean temperatures (an important control on opal dissolution rate) are made more realistic by modifying the temperature of

convectively unstable (vertical) intervals by a weighted averaging with ocean surface properties [Ridgwell, 2001]. This could be thought of as equivalent to the effect of a sinking plume of cold, dense surface water, mixing with its surroundings as it sinks.

3. High vertical mixing rates – Generally enhanced vertical mixing in the Southern Ocean (i.e., associated with frontal systems and other subgrid scale processes) is accounted for by prescribing increased vertical diffusivity in this region (equivalent to a volumetric exchange of 50 Sv at 62.5°S, and 10 Sv at 51.25°S).

A2.4. Surface Ocean Boundary Conditions

[81] Boundary conditions at the ocean surface are derived from observational data sets; annual mean sea surface temperature is derived from *Levitus et al.* [1994b] (at 30 m depth), salinity is taken from *Levitus et al.* [1994a] (but modified in the southernmost grid cell following *Stocker and Wright* [1996]), and annual mean wind speed field is derived from *Trenberth et al.* [1989].

A3. Ocean Biogeochemical Cycling

A3.1. Biological New Production

[82] Numerous mechanistic schemes for representing biological productivity in the surface ocean and based on multi-component descriptions of ecosystem structure and nutrient cycling have been developed to date [e.g., *Aksnes et al.*, 1995; *Andersen et al.*, 1987; *Fasham et al.*, 1990]. Although a few of such schemes have been incorporated into global ocean carbon cycle models, their computational demands make their use in extended model integrations problematic. Much simpler is to estimate a value for new (export) production directly from available surface nutrient concentrations, a tactic used in many carbon cycle models [e.g., *Archer et al.*, 2000b; *Heinze et al.*, 1999; *Maier-Reimer*, 1993]. This is the approach we adopt here. However, in contrast to studies where total POM export is estimated first, and only subsequently are the effects of ecosystem composition in determining various particulate matter “rain ratios” taken into account, we distinguish POM export production arising from different classes of phytoplankton at a much lower level. We make the division between two distinct classes of phytoplankton following the observations of *Egge and Aksnes* [1992]; siliceous phytoplankton (designated hereafter “SP”) and nonsiliceous phytoplankton (“NSP”). SP (typified by open ocean diatom species such as *Thalassiosira oceanica*) are assumed to be solely responsible for the production of opal, and as a result are limited by the availability of H_4SiO_4 . In contrast, NSP (typified by open ocean coccolithophorids such as *Emiliania huxleyi*, but including the bulk of pico- and nanophytoplankton species), have no such silicic acid limitation and are assumed to include the sole producers of $CaCO_3$. Both classes are affected by ambient concentrations of PO_4 and Fe, temperature, and light. In the absence of any nutrient limitation (and assuming a stable water column and adequate insolation levels), siliceous phytoplanktons tend to dominate the phytoplankton community [Egge, 1998]. SP are therefore characterized in the model by a relatively high net (export) productivity. NSP tend to generally comprise somewhat smaller species with productivity

much more tightly controlled by grazing, and are therefore characterized by relatively low net productivity. Obviously this is highly simplistic, with no explicit account taken of the role played by zooplankton or of the microbial loop [Taylor and Joint, 1990]. In addition, the contribution made to total POM export by high productivity nonsiliceous bloom-forming species such as *Phaeocystis antarctica* in regions such as the Southern Ocean will not be captured. However, this scheme is still able to capture the first order contrast in the observed calcium carbonate to particulate organic carbon ($CaCO_3:POC$) rain ratio between different oceanic regions [Ridgwell, 2001].

[83] It is worth noting that in contrast to the assumptions of our “biological” scheme, which is based on nutrient limitation by PO_4 , H_4SiO_4 , and Fe, present-day surface nutrient distributions [Conkright et al., 1994] suggest that the availability of nitrate (NO_3) is likely to be generally more limiting to phytoplankton growth than PO_4 [McElroy, 1983; Tyrrell, 1999]. Because of the complexity of the oceanic NO_3 cycle, and the importance of localized anoxic zones for denitrification (poorly resolved features in our model), no explicit representation is made of the operation of this nutrient cycle. However, the contribution made to alkalinity partitioning in the ocean by NO_3 cycled through the “soft tissue pump” [Broecker and Peng, 1982] is still taken into account.

A3.2. Phosphate Uptake Model

[84] Net uptake fluxes (in units of $mol\ PO_4\ kg^{-1}\ a^{-1}$) within the euphotic zone by siliceous phytoplankton ($u_{SP}^{PO_4}$) and nonsiliceous phytoplankton ($u_{NSP}^{PO_4}$) are based on the “law of the minimum” for multiple nutrient limitation [Aksnes et al., 1994], and described by

$$u_{SP}^{PO_4} = u_{0,SP}^{PO_4} \text{MIN}(k_{SP}^{PO_4}, k_{SP}^{H_4SiO_4}, k_{SP}^{Fe}) \mu_{(I)} \mu_{(T)} \quad (A2a)$$

$$u_{NSP}^{PO_4} = u_{0,NSP}^{PO_4} \text{MIN}(k_{NSP}^{PO_4}, k_{NSP}^{Fe}) \mu_{(I)} \mu_{(T)} \quad (A2b)$$

where $u_{0,SP}^{PO_4}$ and $u_{0,NSP}^{PO_4}$ are uptake rates ($mol\ PO_4\ kg^{-1}\ a^{-1}$) in the absence of any nutrient limitation and treated as “optimizable” parameters – values of 5.00 and 0.25 $\mu mol\ PO_4\ kg^{-1}\ a^{-1}$, for SP and NSP, respectively, are chosen [Ridgwell, 2001]. $\mu_{(I)}$ is a factor accounting for the effects ambient solar insolation has on new production, while $\mu_{(T)}$ is similar, but for temperature. A realistic treatment of light limitation is complex, requiring consideration of the depth distribution of phytoplankton in the water column, effects of self-shading and photo-inhibition, and an estimate of the depth of the mixed layer [Andersen et al., 1987; Taylor et al., 1991; Tyrrell and Taylor, 1996], all of which are beyond the scope of the current model. A simple (normalized) insolation factor is therefore used [Ridgwell, 2001]. $\mu_{(T)}$ is defined as

$$\mu_{(T)} = e^{(aT)} \quad (A3)$$

such that $\mu_{(T)}$ takes a value of unity at a temperature of 0°C. A Q_{10} -type dependence is assumed, with the scalar a given by [Aksnes et al., 1995]

$$a = \ln \left(\frac{Q_{10}}{10} \right) \quad (A4)$$

[85] Following *Eppley* [1972], a Q_{10} value for phytoplankton growth of 1.88 is assumed, giving $a = 0.063$. No

Table 6. Nutrient Half-Saturation Constant Values Assumed for the Two Phytoplankton Groups^a

Phytoplankton Group	Nutrient	K_S value (equation (A5))
Siliceous (SP)	PO ₄	0.1 $\mu\text{mol kg}^{-1}$
Siliceous (SP)	H ₄ SiO ₄	4.0 $\mu\text{mol kg}^{-1}$
Siliceous (SP)	Fe	0.125 nmol kg^{-1}
Nonsiliceous (NSP)	PO ₄	0.1 $\mu\text{mol kg}^{-1}$
Nonsiliceous (NSP)	H ₄ SiO ₄	n/a
Nonsiliceous (NSP)	Fe	0.067 nmol kg^{-1}

^a Adapted from the study of *Ridgwell* [2001].

distinction is made between the two different phytoplankton groups in terms of their temperature response [*Aksnes et al.*, 1995].

[86] The “ k ” terms in (equation (A2a)) represent Michaelis-Menten kinetic limitation of uptake [*Aksnes and Egge*, 1991; *Dugdale*, 1967]

$$k_{\text{SP}}^{\text{PO}_4} = \frac{[\text{PO}_4]}{K_{\text{S,SP}}^{\text{PO}_4} + [\text{PO}_4]} \quad (\text{A5a})$$

$$k_{\text{SP}}^{\text{H}_4\text{SiO}_4} = \frac{[\text{H}_4\text{SiO}_4]}{K_{\text{S,SP}}^{\text{H}_4\text{SiO}_4} + [\text{H}_4\text{SiO}_4]} \quad (\text{A5b})$$

$$k_{\text{SP}}^{\text{Fe}} = \frac{[\text{Fe}]}{K_{\text{S,SP}}^{\text{Fe}} + [\text{Fe}]} \quad (\text{A5c})$$

where K_S values in the three equations are the half-saturation constants for the respective nutrients. The NSP terms are similar, except that there is no H₄SiO₄ limitation. Phytoplankton nutrient half-saturation constants are derived from values observed in incubation and whole-ocean ecosystem studies, as detailed by *Ridgwell* [2001]. Assumed values are summarized in Table 6.

[87] Strictly speaking, Michaelis-Menten limitation kinetics and the associated use of half-saturation constants are not directly applicable to a model of this type. Reported constants are calculated on the basis of the growth rate of individual phytoplankton cells, whereas our model attempts to predict net nutrient removal throughout the euphotic zone (taken to be equal to export production). It is likely that export production has no simple relationship with primary production [*Aksnes and Wassmann*, 1993]. However, for want of a suitable alternative, this concise and easily interpretable parameterization is adopted here.

[88] Integrating net uptake (equations (A2a) and (A2b)) over the depth of the euphotic zone ($D_{\text{euph}} = 50$ m) and total ice-free area, gives the total net uptake rate from each oceanic region (in units of $\text{mol PO}_4 \text{ a}^{-1}$)

$$U_{\text{SP}}^{\text{PO}_4} = u_{\text{SP}}^{\text{PO}_4} 1027 A^{\text{tot}} (1 - A_f^{\text{ice}}) D_{\text{euph}} \quad (\text{A6a})$$

$$U_{\text{NSP}}^{\text{PO}_4} = u_{\text{NSP}}^{\text{PO}_4} 1027 A^{\text{tot}} (1 - A_f^{\text{ice}}) D_{\text{euph}} \quad (\text{A6b})$$

where the mean density of sea water is assumed to be 1027 kg m^{-3} , and A^{tot} is the total surface area (m^2). Finally, (steady state) export production out of the euphotic zone (Fnp) is simply set equal to the net uptake rate (equations (A6a) and (A6b)).

A3.3. “Redfield” and Other Chemical Export Ratios

[89] While equations (A6a) and (A6b) together predict the particulate PO₄ flux, export of other biogeochemically

important nutrient, and nonnutrient chemical species, such as H₄SiO₄, Fe, CO₂, and alkalinity (from Ca²⁺ and NO₃⁻) must be derived. The organic or inorganic components of particulate matter export are related directly (or via an intermediary) to phosphate export, by a series of characteristic ratios. For SP, these relationships are

$$Fnp_{\text{SP}}^{\text{POC}} = r_{\text{SP}}^{\text{POC:POP}} Fnp_{\text{SP}}^{\text{POP}} \quad (\text{A7a})$$

$$Fnp_{\text{SP}}^{\text{ALK}} = -0.7 r_{\text{SP}}^{\text{PON:POP}} Fnp_{\text{SP}}^{\text{POP}} \quad (\text{A7b})$$

$$Fnp_{\text{SP}}^{\text{POFe}} = r_{\text{SP}}^{\text{POFe:POP}} Fnp_{\text{SP}}^{\text{POP}} \quad (\text{A7c})$$

$$Fnp_{\text{SP}}^{\text{opal}} = r_{\text{SP}}^{\text{opal:POP}} Fnp_{\text{SP}}^{\text{POP}} \quad (\text{A7d})$$

where $r_{\text{SP}}^{x,y}$ is a molar ratio linking particulate constituent x to (particulate constituent) y , and POP, PON, and POFe are the PO₄, NO₃, and Fe components of particulate organic matter, respectively. For NSP, they are

$$Fnp_{\text{NSP}}^{\text{POC}} = r_{\text{NSP}}^{\text{POC:POP}} Fnp_{\text{NSP}}^{\text{POP}} \quad (\text{A8a})$$

$$Fnp_{\text{NSP}}^{\text{ALK}} = -0.7 r_{\text{NSP}}^{\text{PON:POP}} Fnp_{\text{NSP}}^{\text{POP}} + 2 r_{\text{NSP}}^{\text{CaCO}_3:\text{POC}} Fnp_{\text{NSP}}^{\text{POC}} \quad (\text{A8b})$$

$$Fnp_{\text{NSP}}^{\text{POFe}} = r_{\text{NSP}}^{\text{POFe:POP}} Fnp_{\text{NSP}}^{\text{POP}} \quad (\text{A8c})$$

and with an additional (inorganic) carbon flux associated with CaCO₃. The proportions of C and N to P in POM are characterized by observed mean ratios (the so-called “Redfield” ratios), with $r^{\text{POC:POP}}$ and $r^{\text{PON:POP}}$ taking values of 106:1 and 16:1, respectively [*Redfield et al.*, 1963]. The same ratios are assumed for POM derived from both SP and NSP. Export ratios of Fe:C in organic matter differ between SP and NSP, and also vary as a function of ambient (total) dissolved Fe concentrations – described by *Ridgwell* [2001] and *Watson et al.* [2000].

[90] The export ratio of CaCO₃:POC from nonsiliceous phytoplankton ($r_{\text{NSP}}^{\text{CaCO}_3:\text{POC}}$) is left as an optimizable parameter in the model – a value of 0.3 is found to allow a reasonable global distribution of CaCO₃ in deep-sea sediments [*Ridgwell*, 2001]. While the value of is itself invariant and spatially uniform, the net CaCO₃:POC export ratio at any one location in time and space comprises export from both SP (contributing POC only) and NSP (contributing both POC and CaCO₃). Temporal or spatial variability in the balance between SP and NSP productivity (for instance, due to changes in the availability of H₄SiO₄) can thus give rise to variability in the net CaCO₃:POC export ratio. The result is that characteristic regional present-day CaCO₃:POC ratios observed in settling particulate matter [*Tsunogai and Noriki*, 1991] can be reproduced in the model, at least to a first-order [*Ridgwell*, 2001].

[91] Incubation and ocean patch studies have reported changes in the cellular H₄SiO₄:C uptake ratio by phytoplankton assemblages upon addition of iron [*Hutchins and Bruland*, 1998; *Takeda*, 1998; *Watson et al.*, 2000]. Fe-stressed diatoms are also visibly more heavily silicified [*Hutchins et al.*, 1998; *Leynaert et al.*, 1993]. This increase in diatom ratio H₄SiO₄:C with decreasing Fe-availability has been suggested to be due to the order of cell cycle events, where silicic acid uptake only occurs in a phase just prior to cellular division [*Pondaven et al.*, 1999]. If division is delayed through Fe-limitation, the length of time avail-

able for opal deposition is longer, thus resulting in a higher degree of diatom silicification. If this is the case, a reasonable starting point in relating $\text{H}_4\text{SiO}_4\text{:C}$ uptake to ambient would be to assume that this ratio is proportional to Fe-stress as defined by the reciprocal of the relevant Michaelis-Menten kinetic term (equation A5c), giving

$$r_{\text{SP}}^{\text{H}_4\text{SiO}_4\text{:C}} = r_{0,\text{SP}}^{\text{H}_4\text{SiO}_4\text{:C}} \frac{1}{k^{\text{Fe}}} \quad (\text{A9})$$

where $r_{0,\text{SP}}^{\text{H}_4\text{SiO}_4\text{:C}}$ is the ratio of $\text{H}_4\text{SiO}_4\text{:C}$ uptake under Fe-replete conditions. The singularity at $[\text{Fe}] = 0$ is removed by adding a fixed offset ($[\text{Fe}]_{\text{off}}$) to the value of ambient $[\text{Fe}]$. Observed decreases in diatom $\text{H}_4\text{SiO}_4\text{:C}$ with increasing Fe availability [Hutchins and Bruland, 1998; Takeda, 1998; Watson et al., 2000] can be reasonably reproduced with $K_S^{\text{Kc}} = 0.25 \text{ nmol kg}^{-1}$ and $[\text{Fe}]_{\text{off}} = 0.125 \text{ nmol kg}^{-1}$ [Ridgwell, 2001].

[92] Given their very different biogeochemical natures, a high degree of differential recycling between opal and POC within the euphotic zone is likely [Dugdale et al., 1995; Dugdale and Wilkerson, 1998]. Changes in the degree of diatom silicification may alter the magnitude of this differential, such as through changes in sinking rate [Boyle, 1998; Muggli et al., 1996], grazing susceptibility, or the “quality” of frustuline opal (and thus solubility and/or dissolution rate). However, for simplicity, the export opal:POC ratio ($r_{\text{SP}}^{\text{opal:POC}}$) will be assumed to scale linearly with the cellular $\text{H}_4\text{SiO}_4\text{:C}$ uptake ratio. The export ratio can therefore be written as

$$r_{\text{SP}}^{\text{opal:POC}} = r_{0,\text{SP}}^{\text{opal:POC}} \frac{K_S^{\text{Fe}} + ([\text{Fe}] + [\text{Fe}]_{\text{off}})}{([\text{Fe}] + [\text{Fe}]_{\text{off}})} \quad (\text{A10})$$

where $r_{0,\text{SP}}^{\text{opal:POC}}$ is now the opal:POC export ratio under Fe-replete conditions. The magnitude of differential recycling within the euphotic zone represented by the implicit scale factor linking $r_{0,\text{SP}}^{\text{opal:POC}}$ to $r_{0,\text{SP}}^{\text{H}_4\text{SiO}_4\text{:C}}$ is poorly quantified, and has been variously estimated to be in the range from 1.25 to 3.0 depending on assumptions made regarding grazing [Dugdale et al., 1995; Dugdale and Wilkerson, 1998]. $r_{0,\text{SP}}^{\text{opal:POC}}$ is therefore left as a final optimizable parameter in the model – a reasonable value being found to be $0.175 \text{ mol mol}^{-1}$ [Ridgwell, 2001], equivalent to a plausible value of differential recycling value of 1.5.

A3.4. Remineralization Within the Ocean Interior

[93] Nutrients, DIC, and ALK, can all be removed from solution in the euphotic zone through biological action, and exported in particulate form (POM, CaCO_3 , and opal) to the depth. Remineralization of biogenic material and release of dissolved constituent species are represented as processes occurring instantaneously throughout the ocean interior. For POM, remineralization is assumed to occur according to a simple power law distribution [Ridgwell, 2001], with no fractionation taking place between the different nutrients or with carbon, and no differentiation made between POM derived from SP and that from NSP. CaCO_3 is assumed to be remineralized in a similar manner as described by Archer et al. [1998] and Ridgwell [2001], while opal remineralization proceeds as detailed earlier (section 2.2). Remineralization is allowed to occur everywhere in the ocean at water depths below 100 m, with the exception of the equatorial

upwelling zones of each basin, notorious regions for modeling problems related to “nutrient trapping” [Najjar et al., 1992]. To alleviate nutrient trapping in these regions, the depth at which remineralization begins is artificially deepened; 400 m in the equatorial Atlantic and Pacific and 200 m in the equatorial Indian Ocean [Ridgwell, 2001]. This “topological fix” is employed as an alternative to the prescription of a high proportion of organic new production in dissolved form – the more traditional “fix” used in an attempt to counter the biogeochemical consequences of spatial resolution insufficient to adequately resolve complex upwelling systems [Marchal et al., 1998b; Najjar et al., 1992; Yamanaka and Tajika, 1997].

A3.5. Iron Biogeochemical Cycling

[94] The cycling of dissolved iron in the ocean (considered to be in the form of a single bioavailable species) follows previous studies [Ridgwell et al., 2002; Watson et al., 2000], with the parameterization of variable (ambient $[\text{Fe}]$ -dependent) Fe:C uptake ratios and scavenging by biogenic material settling through the water column accounted for [Ridgwell, 2001; Watson et al., 2000]. The effect of dust loading at the surface ocean on the effective solubility of aeolian Fe [Chester et al., 1993; Spokes and Jickells, 1996; Zhaung et al., 1990] is also taken into account by parameterizing the re-absorption of Fe onto dust particles – “self-scavenging” [Ridgwell, 2001].

A4. Ocean Sediments

[95] The Bern OGCM [Stocker and Wright, 1996] assumes a uniform ocean depth of 4000 m. However, to correctly represent the interaction between ocean and deep-sea sediments, variations in the depth of the ocean floor must be taken into account [Keir, 1995]. A bathymetric profile (defining the mean global distribution of fractional ocean floor area with depth [ETOPO5, 1988]) is assumed at each of the 16 ocean grid points of the model. To retain relative ocean cell volumes, ocean layer thickness is adjusted to give lower boundary depths of 47, 95, 144, 496, 1013, 2652, 3986, and 6000 m, while to preserve total ocean volume the width of each ocean basin is increased by $\sim 9\%$.

[96] The continuous bathymetric profile is discretized into a series of separate depth bands, each of which is associated with an individual module handling ocean-sediment interactions [Munhoven and Francois, 1994, 1996; Sundquist, 1990; Walker and Opdyke, 1995], as shown in Figure 1. Fifteen discrete sediment levels are considered, which between them span the depth of the ocean interior from 6000 m up to base of the euphotic zone (100 m), thus giving a total of separate 240 sedimentary modules (i.e., 15 for each of the 16 ocean grid points) [Ridgwell, 2001]. These sediment modules are similar in configuration and (physical) operation to those employed by Munhoven and Francois [1994, 1996] and Walker and Opdyke [1995]. They comprise a single (10 cm thick) surface layer, underlain by a series of (1 cm thick) sublayers. The surface layer represents the upper zone of the sediment where bioturbation effectively homogenizes solid composition, and where the primary diagenetic processes take place. Excess solid material is exported out of this surface layer (i.e., “buried”) and stored in a stack of sedimentary sublayers lying immedi-

ately below. In addition to the advective transfer of solids between the surface layer and the stack (arising from net sedimentary accumulation/erosion) a diffusive-like transfer is prescribed between the uppermost sublayers, representing deeper, less intense bioturbation. Further details are given by Ridgwell [2001].

[97] Solid components represented in the sediments include CaCO_3 (as calcite) and opal, all of which share a biogenic origin in the surface ocean and whose fractional preservation in the sediments is explicitly calculated. The diagenesis (dissolution) of calcite is parameterized following the method of Archer [1991], while opal dissolution is predicted with the scheme presented in this article (section 2.1). Deposition on the sediments of detrital matter derived from aeolian deposition at the ocean surface also takes place. However, unlike the biogenic components, detrital matter is assumed to act conservatively within the sediments, with no release of either H_4SiO_4 (from silicates) or dissolved Fe (from Fe-bearing ore and silicate minerals). Finally, a mean fractional preservation of the POC settling flux of 5% is assumed, consistent with estimates of $\sim 3\text{--}7\%$ [Archer et al., 2002; Tromp et al., 1995].

[98] **Acknowledgments.** This work was supported by a UK Natural Research Council Ph.D. grant to A.J.R. We would like to thank Paul Tréguer and an anonymous reviewer, whose thorough and thoughtful review has led to significant improvements to this paper.

References

- Aksnes, D. L., and J. K. Egge, A theoretical-model for nutrient-uptake in phytoplankton, *Mar. Ecol. Prog. Ser.*, **70**, 65–72, 1991.
- Aksnes, D. L., and P. Wassmann, Modeling the significance of zooplankton grazing for export production, *Limnol. Oceanogr.*, **38**, 978–985, 1993.
- Aksnes, D. L., J. K. Egge, R. Rosland, and B. R. Heimdal, Representation of *Emiliania huxleyi* in phytoplankton simulation models – A 1st approach, *Sarsia*, **79**, 291–300, 1994.
- Aksnes, D. L., K. B. Ulvestad, B. M. Balino, J. Berntsen, J. K. Egge, and E. Svendsen, Ecological modeling in coastal waters – towards predictive physical-chemical-biological simulation-models, *Ophelia*, **41**, 5–36, 1995.
- Andersen, V., P. Nival, and R. P. Harris, Modelling of a phytoplankton ecosystem in an enclosed water column, *J. Mar. Biol. Assoc. U.K.*, **67**, 407–430, 1987.
- Archer, D., Modeling the calcite lysocline, *J. Geophys. Res.*, **96**, 17,037–17,050, 1991.
- Archer, D., A data-driven model of the global calcite lysocline, *Global Biogeochem. Cycles*, **10**, 511–526, 1996.
- Archer, D., and E. Maier-Reimer, Effect of deep-sea sedimentary calcite preservation on atmospheric CO_2 concentration, *Nature*, **367**, 260–263, 1994.
- Archer, D., M. Lyle, K. Rodgers, and P. Froelich, What controls opal preservation in tropical deep-sea sediments, *Paleoceanography*, **8**, 7–21, 1993.
- Archer, D., H. Kheshgi, and E. Maier-Reimer, Multiple timescales for neutralization of fossil fuel CO_2 , *Geophys. Res. Lett.*, **24**, 405–408, 1997.
- Archer, D., H. Kheshgi, and E. Maier-Reimer, Dynamics of fossil fuel CO_2 neutralization by marine CaCO_3 , *Global Biogeochem. Cycles*, **12**, 259–276, 1998.
- Archer, D., G. Eshel, A. Winguth, and W. Broecker, Atmospheric CO_2 sensitivity to the biological pump in the ocean, *Global Biogeochem. Cycles*, **14**, 1219–1230, 2000a.
- Archer, D., A. Winguth, D. Lea, and N. Mahowald, What caused the glacial/interglacial atmospheric $p\text{CO}_2$ cycles?, *Rev. Geophys.*, **38**, 159–189, 2000b.
- Archer, D. E., J. L. Morfoed, and S. R. Emerson, A model of suboxic sedimentary diagenesis suitable for automatic tuning and gridded global domains, *Global Biogeochem. Cycles*, **16**, 1017, 10.1029/2000GB001288, 2002.
- Bacastow, R., and E. Maier-Reimer, Ocean-circulation model of the carbon cycle, *Clim. Dyn.*, **4**, 95–125, 1990.
- Berelson, W. M., Particle settling rates increase with depth in the ocean, *Deep Sea Res.*, **49**, 237–251, 2002.
- Berger, W. H., and E. Vincent, Deep-sea carbonate: Reading the carbon-isotope signal, *Geol. Rundsch.*, **75**, 249–269, 1986.
- Bidle, K. D., and F. Azam, Accelerated dissolution of diatom silica by marine bacterial assemblages, *Nature*, **397**, 508–512, 1999.
- Blain, S., P. Tréguer, and M. Rodier, Stocks and fluxes of biogenic silica in the western oligotrophic equatorial Pacific, *J. Geophys. Res. Oceans*, **104**, 3357–3367, 1999.
- Boyle, E. A., Pumping iron makes thinner diatoms, *Nature*, **393**, 733–734, 1998.
- Broecker, W. S., Glacial to interglacial changes in ocean chemistry, *Prog. Oceanogr.*, **11**, 151–197, 1982.
- Broecker, W. S., and G. M. Henderson, The sequence of events surrounding Termination II and their implications for the cause of glacial-interglacial CO_2 changes, *Paleoceanography*, **13**, 352–364, 1998.
- Broecker, W. S., and T.-H. Peng, *Tracers in the Sea*, Lamont-Doherty Geological Observatory, New York, 1982.
- Broecker, W. S., J. Lynch-Stieglitz, D. Archer, M. Hofmann, E. Maier-Reimer, O. Marchal, T. Stocker, and N. Gruber, How strong is the Harvardton-Bear constraint?, *Global Biogeochem. Cycles*, **13**, 817–820, 1999.
- Brzezinski, M. A., and D. M. Nelson, The annual silica cycle in the Sargasso Sea near Bermuda, *Deep Sea Res.*, **Part I**, **42**, 1215–1237, 1995.
- Charles, C. D., P. N. Froelich, M. A. Zibello, R. A. Mortlock, and J. J. Morley, Biogenic opal in Southern Ocean sediments over the last 450,000 years: Implications for surface water chemistry and circulation, *Paleoceanography*, **6**, 697–728, 1991.
- Chester, R., K. J. T. Murphy, F. J. Lin, A. S. Berry, G. A. Bradshaw, and P. A. Corcoran, Factors controlling the solubilities of trace metals from non-remote aerosols deposited to the sea surface by the dry deposition model, *Mar. Chem.*, **42**, 107–126, 1993.
- CLIMAP project members The surface of the ice-age Earth, *Science*, **191**, 1131–1137, 1976.
- Codispoti, L. A., Is the ocean losing nitrate?, *Nature*, **376**, 724, 1995.
- Conkright, M. E., S. Levitus, and T. P. Boyer, *World Ocean Atlas 1994*, vol. 1, *Nutrients*, NOAA Atlas NESDIS 1, p.150, U.S. Dept. of Commerce, Washington, D. C., 1994.
- DeMaster, D. J., The supply and accumulation of silica in the marine environment, *Geochim. Cosmochim. Acta*, **45**, 1715–1732, 1981.
- DeMaster, D. J., The accumulation and cycling of biogenic silica in the Southern Ocean: Revisiting the marine silica budget, *Deep Sea Res.*, **49**, 3155–3167, 2002.
- DeMenocal, P. B., W. F. Ruddiman, and E. M. Pokras, Influences of high-latitude and low-latitude processes on African terrestrial climate – Pleistocene eolian records from equatorial Atlantic Ocean Drilling Program Site 663, *Paleoceanography*, **8**, 209–242, 1993.
- Dixit, S., P. Van Cappellen, and A. J. van Bennekom, Processes controlling solubility of biogenic silica and pore water build-up of silicic acid in marine sediments, *Mar. Chem.*, **73**, 333–352, 2001.
- Duce, R. A., et al., The atmospheric input of trace species to the world ocean, *Global Biogeochem. Cycles*, **5**, 193–259, 1991.
- Dugdale, R. C., Nutrient limitation in the sea: Dynamics, identification, and significance, *Limnol. Oceanogr.*, **12**, 685–695, 1967.
- Dugdale, R. C., and F. P. Wilkerson, Silicate regulation of new production in the equatorial Pacific upwelling, *Nature*, **391**, 270–273, 1998.
- Dugdale, R. C., F. P. Wilkerson, and H. J. Minas, The role of silicate pump in driving new production, *Deep Sea Res.*, **Part I**, **42**, 697–719, 1995.
- Egge, J. K., Are diatoms poor competitors at low phosphate concentrations?, *J. Mar. Syst.*, **16**, 191–198, 1998.
- Egge, J. K., and D. L. Aksnes, Silicate as regulating nutrient in phytoplankton competition, *Mar. Ecol. Prog. Ser.*, **83**, 281–289, 1992.
- Emerson, S., and M. Bender, Carbon fluxes at the sediment-water interface of the deep-sea: Calcium carbonate preservation, *J. Mar. Res.*, **39**, 139–162, 1981.
- Eppley, R. W., Temperature and phytoplankton growth in the sea, *Fish. Bull.*, **70**, 1063–1085, 1972.
- Erez, J., K. Takahashi, and S. Honjo, In-situ dissolution experiment of Radiolaria in the central North Pacific Ocean, *Earth Planet. Sci. Lett.*, **59**, 245–254, 1982.
- ETOPO5, Data Announcement 88-MGG-02, *Digital relief of the Surface of the Earth*, NOAA, National Geophysical Data Centre, Westview, Boulder, Colo., 1988.
- Fairbanks, R. G., A 17,000-year glacio-eustatic sea level record: Influence of glacial melting rates on the Younger Dryas event and deep-ocean circulation, *Nature*, **342**, 637–642, 1989.
- Fasham, M. J. R., H. W. Ducklow, and S. M. McKelvie, A nitrogen-based model of plankton dynamics in the oceanic mixed layer, *J. Mar. Res.*, **48**, 591–639, 1990.

- Gnanadesikan, A., A global model of silicon cycling: Sensitivity to eddy parameterization and dissolution, *Global Biogeochem. Cycles*, *13*, 199–220, 1999.
- Hales, B., and S. Emerson, Evidence in support of first-order dissolution kinetics of calcite in seawater, *Earth Planet. Sci. Lett.*, *148*, 317–327, 1997.
- Harrison, K. G., Role of increased marine silica input on paleo- $p\text{CO}_2$ levels, *Paleoceanography*, *15*, 292–298, 2000.
- Heinze, C., and T. J. Crowley, Sedimentary response to ocean gateway circulation changes, *Paleoceanography*, *12*, 742–754, 1997.
- Heinze, C., E. Maier-Reimer, A. M. E. Winguth, and D. Archer, A global oceanic sediment model for long-term climate studies, *Global Biogeochem. Cycles*, *13*, 221–250, 1999.
- Hensen, C., H. Landenberger, M. Zabel, and H. D. Schulz, Quantification of diffusive benthic fluxes of nitrate, phosphate, and silicate in the southern Atlantic Ocean, *Global Biogeochem. Cycles*, *12*, 193–210, 1998.
- Holtstag, A. A. M., and A. P. VanUlden, A simple scheme for daytime estimates of the surface fluxes from routine weather data, *J. Clim. Appl. Meteorol.*, *22*, 517–529, 1983.
- Honjo, S., Material fluxes and modes of sedimentation in the mesopelagic and bathypelagic zones, *J. Mar. Res.*, *38*, 53–97, 1980.
- Honjo, S., and S. J. Manganini, Annual biogenic particulate fluxes to the interior of the north Atlantic Ocean studies at 34°N 21°W and 48°N 21°W, *Deep Sea Res., Part II*, *40*, 587–607, 1993.
- Honjo, S., S. J. Manganini, and J. J. Cole, Sedimentation of biogenic matter in the deep ocean, *Deep Sea Res.*, *29*, 609–625, 1982.
- Houghton, J. T., et al. (Eds.), *Climate Change 2001: The Scientific Basis. Contribution of Working Group I to the Third Assessment Report of the Intergovernmental Panel on Climate Change*, Cambridge Univ. Press, New York, 2001.
- Hovine, S., and T. Fichefet, A zonally averaged 3-basin ocean circulation model for climate studies, *Clim. Dyn.*, *10*, 313–331, 1994.
- Hutchins, D. A., and K. W. Bruland, Iron-limited diatom growth and Si:N uptake ratios in a coastal upwelling regime, *Nature*, *393*, 561–564, 1998.
- Hutchins, D. A., G. R. DiTullio, Y. Zhang, and K. W. Bruland, An iron limitation mosaic in the California upwelling regime, *Limnol. Oceanogr.*, *43*, 1037–1054, 1998.
- Imbrie, J., et al., The orbital theory of Pleistocene climate: Support from a revised chronology of the marine record, in *Milankovitch and Climate, Part I*, edited by A. Berger et al., Norwell, Mass., 1984.
- Jones, I. W., G. Munhoven, M. Tranter, P. Huybrechts, and M. J. Sharp, Modelled glacial and non-glacial HCO_3^- , Si and Ge fluxes since the LGM: little potential for impact on atmospheric CO_2 concentrations and a potential proxy of continental chemical erosion, the marine Ge/Si ratio, *Global Planet. Change*, *33*, 139–153, 2002.
- Kamatani, A., Dissolution rates of silica from diatoms decomposing at various temperatures, *Mar. Biol.*, *68*, 91–96, 1982.
- Keir, R. S., The dissolution kinetics of biogenic calcium carbonates in seawater, *Geochim. Cosmochim. Acta*, *44*, 241–252, 1980.
- Keir, R. S., Is there a component of Pleistocene CO_2 change associated with carbonate dissolution cycles?, *Paleoceanography*, *10*, 871–880, 1995.
- Kumar, N., R. F. Anderson, R. A. Mortlock, P. N. Froelich, P. Kubik, and M. Suter, Increased biological productivity and export production in the glacial Southern Ocean, *Nature*, *378*, 675–680, 1995.
- Levitus, S., and T. P. Boyer, *World Ocean Atlas 1994*, vol. 4, *Temperature*, NOAA Atlas NESDIS 4, p. 117, U.S. Dept. of Commerce, Washington, D. C., 1994.
- Levitus, S., R. Burgett, and T. P. Boyer, *World Ocean Atlas 1994*, vol. 3, *Salinity*, NOAA Atlas NESDIS 3, p. 99, U.S. Dept. of Commerce, Washington, D. C., 1994.
- Leynaert, A., D. M. Nelson, B. Queguiner, and P. Treguer, The silica cycle in the antarctic ocean – is the Weddell sea atypical, *Mar. Ecol. Prog. Ser.*, *96*, 1–15, 1993.
- Maher, B. A., and P. F. Dennis, Evidence against dust-mediated control of glacial-interglacial changes in atmospheric CO_2 , *Nature*, *411*, 176–180, 2001.
- Maier-Reimer, E., Geochemical cycles in an ocean general circulation model. Pre-industrial tracer distributions, *Global Biogeochem. Cycles*, *7*, 645–677, 1993.
- Mahowald, N., K. Kohfeld, M. Hansson, Y. Balkanski, S. P. Harrison, I. C. Prentice, M. Schulz, and H. Rodhe, Dust sources and deposition during the last glacial maximum and current climate: A comparison of model results with paleodata from ice cores and marine sediments, *J. Geophys. Res.*, *104*, 15,895–15,916, 1999.
- Marchal, O., T. F. Stocker, and F. Joos, Impact of oceanic reorganizations on the ocean carbon cycle and atmospheric carbon dioxide content, *Paleoceanography*, *13*, 225–244, 1998a.
- Marchal, O., T. F. Stocker, and F. Joos, A latitude-depth, circulation bio-geochemical ocean model for paleoclimate studies. Development and sensitivities, *Tellus, Ser. B*, *50*, 290–316, 1998b.
- Marchal, O., T. F. Stocker, F. Joos, A. Indermuhle, T. Blunier, and J. Tschumi, Modelling the concentration of atmospheric CO_2 during the Younger Dryas climate event, *Clim. Dyn.*, *15*, 341–354, 1999.
- Martin, W. R., M. Bender, M. Leinen, and J. Orcharado, Benthic organic carbon degradation and biogenic silica dissolution in the central equatorial Pacific, *Deep Sea Res., Part I*, *12*, 1481–1516, 1991.
- McElroy, M. B., Marine biological controls on atmospheric CO_2 and climate, *Nature*, *302*, 328–329, 1983.
- McManus, J., D. E. Hammond, W. M. Berelson, T. E. Kilgore, D. J. Demaster, O. G. Ragueneau, and R. W. Collier, Early diagenesis of biogenic opal – Dissolution rates, kinetics, and paleoceanographic implications, *Deep Sea Res., Part II*, *42*, 871–903, 1995.
- Michel, E., L. D. Labeyrie, J. C. Duplessy, N. Gorfli, M. Labracherie, and J. L. Turon, Could deep sub-Antarctic convection feed the world deep basins during the Last Glacial Maximum, *Paleoceanography*, *10*, 927–941, 1995.
- Mortlock, R. A., C. D. Charles, P. N. Froelich, M. A. Zibello, J. Saltzman, J. D. Hays, and L. H. Burckle, Evidence for lower productivity in the Antarctic Ocean during the last glaciation, *Nature*, *351*, 220–222, 1991.
- Muggli, D. L., M. Lecourt, and P. J. Harrison, Effects of iron and nitrogen source on the sinking rate, physiology and metal composition of an oceanic diatom from the subarctic Pacific, *Mar. Ecol. Prog. Ser.*, *132*, 215–227, 1996.
- Munhoven, G., and L. M. Francois, Glacial-interglacial changes in continental weathering: Possible implications for atmospheric CO_2 , in *Carbon Cycling in the Glacial Ocean: Constraints on the Ocean's Role in Global Change*, edited by R. Zahn et al., Springer-Verlag, New York, 1994.
- Munhoven, G., and L. M. Francois, Glacial-interglacial variability of atmospheric CO_2 due to changing continental silicate rock weathering: A model study, *J. Geophys. Res.*, *101*, 21,423–21,437, 1996.
- Najjar, R. G., J. L. Sarmiento, and J. R. Toggweiler, Downward transport and fate of organic matter in the ocean: Simulations with a General Circulation Model, *Global Biogeochem. Cycles*, *6*, 45–76, 1992.
- Nelson, D. M., J. J. Goering, S. S. Kilham, and R. R. L. Guillard, Kinetics of silicic acid uptake and rates of silica dissolution in the marine diatom *Thalassiosira pseudonana*, *J. Phycol.*, *12*, 246–252, 1976.
- Nelson, D. M., P. Treguer, M. A. Brzezinski, A. Leynaert, and B. Queguiner, Production and dissolution of biogenic silica in the ocean: Revised global estimates, comparison with regional data and relationship to biogenic sedimentation, *Global Biogeochem. Cycles*, *9*, 359–372, 1995.
- Noriki, S., and S. Tsunogai, Particulate fluxes and major components of settling particles from sediment trap experiments in the Pacific Ocean, *Deep Sea Res.*, *33*, 903–912, 1986.
- Officer, C. B., and J. H. Ryther, The possible importance of silicon in marine eutrophication, *Mar. Ecol. Prog. Ser.*, *3*, 83–91, 1980.
- Peng, T.-H., and W. S. Broecker, Distribution of ^{32}Si in the world ocean: Model compared to observation, *Global Biogeochem. Cycles*, *7*, 463–474, 1993.
- Petit, J. R., et al., Climate and atmospheric history of the past 420000 years from the Vostok ice core, Antarctica, *Nature*, *399*, 429–436, 1999.
- Pondaven, P., C. Fravallo, D. Ruiz-Pino, P. Treguer, B. Queguiner, and C. Jeandel, Modelling the silica pump in the Permanently Open Ocean Zone of the Southern Ocean, *J. Mar. Syst.*, *17*, 587–619, 1998.
- Pondaven, P., D. Ruiz-Pino, J. N. Druon, C. Fravallo, and P. Treguer, Factors controlling silicon and nitrogen biogeochemical cycles in high nutrient, low chlorophyll systems (the Southern Ocean and the North Pacific): Comparison with a mesotrophic system (the North Atlantic), *Deep Sea Res., Part I*, *46*, 1923–1968, 1999.
- Pondaven, P., O. Ragueneau, P. Treguer, A. Hauvespre, Dezileau, and J.-L. Reyss, Resolving the “opal paradox” in the Southern Ocean, *Nature*, *405*, 168–172, 2000.
- Rabouille, C., and J. F. Gaillard, The validity of steady-state flux calculations in early diagenesis – A computer simulation of deep-sea silica diagenesis, *Deep Sea Res., Part I*, *37*, 625–646, 1990.
- Rabouille, C., J. F. Gaillard, P. Treguer, and M. A. Vincendeau, Biogenic silica recycling in surficial sediments across the Polar Front of the Southern Ocean (Indian Sector), *Deep Sea Res., Part II*, *44*, 1151–1176, 1997.
- Ragueneau, O., et al., A review of the Si cycle in the modern ocean: Recent progress and missing gaps in the application of biogenic opal as a paleo-productivity proxy, *Global Planet. Change*, *26*, 317–365, 2000.
- Rea, D. K., Aspects of atmospheric circulation – The late Pleistocene (0–950,000 yr) record of eolian deposition in the Pacific Ocean, *Palaeogeogr. Palaeoclim. Palaeoecol.*, *78*, 217–227, 1990.
- Redfield, A. C., B. H. Ketchum, and F. A. Richards, The influence of organisms in the composition of sea water, in *The Sea*, edited by N. M. Hill, pp. 26–77, Wiley-Interscience, New York, 1963.

- Rich, J. J., D. Hollander, and G. E. Birchfield, Role of regional bioproductivity in atmospheric CO₂ changes, *Global Biogeochem. Cycles*, **13**, 531–553, 1999.
- Rickert, D., M. Schlüter, and K. Wallmann, Dissolution kinetics of biogenic silica from the water column to the sediments, *Geochim. Cosmochim. Acta*, **66**, 439–455, 2002.
- Ridgwell, A. J., Glacial-interglacial perturbations in the global carbon cycle, Ph.D. thesis, Univ. of East Anglia, Norwich, UK, 2001. (Available at http://tracer.env.uea.ac.uk/e114/ridgwell_2001.pdf).
- Ridgwell, A. J., M. A. Maslin, and A. J. Watson, Reduced effectiveness of terrestrial carbon sequestration due to an antagonistic response of ocean productivity, *Geophys. Res. Lett.*, **29**(6), 1095, 10.1029/2001GL014304, 2002.
- Ridgwell, A. J., and A. J. Watson, Feedback between aeolian dust, climate and atmospheric CO₂ in glacial time, *Paleoceanography*, in press, 2002.
- Sayles, F. L., W. G. Deuser, J. E. Goudreau, W. H. Dickinson, T. D. Jickells, and P. King, The benthic cycle of biogenic opal at the Bermuda Atlantic Time Series site, *Deep Sea Res., Part I*, **43**, 383–409, 1996.
- Schink, D. R., N. L. Guinasso, and K. A. Fanning, Processes affecting the concentration of silica at the sediment-water interface of the Atlantic Ocean, *J. Geophys. Res.*, **80**, 3013–3031, 1975.
- Schluter, M., and E. Sauter, Biogenic silica cycle in surface sediments of the Greenland Sea, *J. Mar. Syst.*, **23**, 333–342, 2000.
- Siegel, D. A., T. C. Granata, A. F. Michaels, and T. D. Dickey, Mesoscale eddy diffusion, particle sinking, and the interpretation of sediment trap data, *J. Geophys. Res.*, **95**, 5305–5311, 1990.
- Six, K. D., and E. Maier-Reimer, Effects of plankton dynamics on seasonal carbon fluxes in an ocean general circulation model, *Global Biogeochem. Cycles*, **10**, 559–583, 1996.
- Smith, H. J., H. Fischer, M. Wahlen, D. Mastroianni, and B. Deck, Dual modes of the carbon cycle since the Last Glacial Maximum, *Nature*, **400**, 248–250, 1999.
- Spokes, L. J., and T. D. Jickells, Factors controlling the solubility of aerosol trace metals in the atmosphere and on mixing into seawater, *Aquat. Geochem.*, **1**, 355–374, 1996.
- Stocker, T. F., and D. G. Wright, Rapid changes in ocean circulation and atmospheric radiocarbon, *Paleoceanography*, **11**, 773–795, 1996.
- Sundquist, E. T., Influence of deep-sea benthic processes on atmospheric CO₂, *Philos. Trans. R. Soc. London, Ser. A*, **331**, 155–165, 1990.
- Takahashi, K., seasonal fluxes of pelagic diatoms in the sub-Arctic Pacific, 1982–1983, *Deep Sea Res., Part I*, **33**, 1225–1251, 1986.
- Takeda, S., Influence of iron availability on nutrient consumption ratio of diatoms in oceanic waters, *Nature*, **393**, 774–777, 1998.
- Taylor, A. H., and I. Joint, A steady-state analysis of the “microbial loop” in stratified systems, *Mar. Ecol. Prog. Ser.*, **59**, 1–17, 1990.
- Taylor, S. R., and S. M. McLennan, *The Continental Crust, its Composition and Evolution: An Examination of the Geochemical Record Preserved in Sedimentary Rocks*, Blackwell, Malden, Mass., 1985.
- Taylor, A. H., A. J. Watson, M. Ainsworth, J. E. Robertson, and D. R. Turner, A modelling investigation of the role of phytoplankton in the balance of carbon at the surface of the North Atlantic, *Global Biogeochem. Cycles*, **5**, 151–171, 1991.
- Tiedemann, R., M. Sarnthein, and N. J. Shackleton, Astronomic timescale for the Pliocene Atlantic d¹⁸O and dust flux records of Ocean Drilling Program site 659, *Paleoceanography*, **9**, 619–638, 1994.
- Tréguer, P., and P. Pondaven, Silica control of carbon dioxide, *Nature*, **406**, 358–359, 2000.
- Tréguer, P., D. M. Nelson, A. J. VanBennekom, D. J. Demaster, A. Leynaert, and B. Queguiner, The silica balance in the world ocean – A re-estimate, *Science*, **268**, 375–379, 1995.
- Trenberth, K., J. Olson, and W. Large, *A Global Ocean Wind Stress Climatology based on ECMWF Analyses*, Tech. Rep. NCAR/TN-338+STR, National Centre for Atmospheric Research, Westview, Boulder, Colo., 1989.
- Tromp, T. K., P. VanCappellen, and R. M. Key, A global model for the early diagenesis of organic carbon and organic phosphorus in marine sediments, *Geochim. Cosmochim. Acta*, **59**, 1259–1284, 1995.
- Tsunogai, S., and S. Noriki, Particulate fluxes of carbonate and organic-carbon in the ocean – is the marine biological activity working as a sink of the atmospheric carbon, *Tellus, Ser. B*, **43**, 256–266, 1991.
- Tyrrell, T., The relative influences of nitrogen and phosphorus on oceanic primary production, *Nature*, **400**, 525–531, 1999.
- Tyrrell, T., and A. H. Taylor, A modelling study of *Emiliania huxleyi* in the NE Atlantic, *J. Mar. Syst.*, **9**, 83–112, 1996.
- Ullman, W. J., and R. C. Aller, Diffusion coefficient in nearshore marine sediments, *Limnol. Oceanogr.*, **27**, 552–556, 1982.
- VanBennekom, A. J., G. W. Berger, S. J. VanDerGaast, and R. T. P. Devries, Primary productivity and the silica cycle in the Southern Ocean (Atlantic sector), *Palaeogeogr. Palaeoclimatol. Palaeoecol.*, **67**, 19–30, 1988.
- VanCappellen, P., and L. Q. Qiu, Biogenic silica dissolution in sediments of the Southern Ocean, 1, Solubility, *Deep Sea Res., Part II*, **44**, 1109–1128, 1997a.
- VanCappellen, P., and L. Q. Qiu, Biogenic silica dissolution in sediments of the Southern Ocean, 2, Kinetics, *Deep Sea Res., Part II*, **44**, 1129–1149, 1997b.
- Walker, J. C. G., and B. C. Opdyke, Influence of variable rates of netiric carbonate deposition on atmospheric carbon dioxide and pelagic sediments, *Paleoceanography*, **10**, 415–427, 1995.
- Watson, A. J., D. C. E. Bakker, A. J. Ridgwell, P. W. Boyd, and C. S. Law, Effect of iron supply on Southern Ocean CO₂ uptake and implications for glacial atmospheric CO₂, *Nature*, **407**, 730–733, 2000.
- Weaver, A. J., and E. S. Sarachik, The role of mixed boundary conditions in numerical models of the oceans climate, *J. Phys. Oceanogr.*, **21**, 1470–1493, 1991.
- Willey, J., Silica-alumina interactions in seawater, *Mar. Chem.*, **3**, 241–251, 1975.
- Wollast, R., and L. Chou, Kinetic study of the dissolution of albite with a continuous flow-through fluidized bed reactor, in *The Chemistry of Weathering*, edited by J. I. Drever and D. Reidel, Norwell, Mass., 1985.
- Yamanaka, Y., and E. Tajika, The role of the vertical fluxes of particulate organic matter and calcite in the oceanic carbon cycle: Studies using an ocean biogeochemical general circulation model, *Global Biogeochem. Cycles*, **10**, 361–382, 1996.
- Yamanaka, Y., and E. Tajika, Role of dissolved organic matter in the marine biogeochemical cycle: Studies using an ocean biogeochemical general circulation-model, *Global Biogeochem. Cycles*, **11**, 599–612, 1997.
- Zhaung, G., R. A. Duce, and D. R. Kester, The dissolution of atmospheric iron in surface seawater of the open ocean, *J. Geophys. Res.*, **95**, 16,207–16,216, 1990.

D. E. Archer, Department of the Geophysical Sciences, University of Chicago, Chicago, IL 60637, USA.

A. J. Ridgwell and A. J. Watson, School of Environmental Sciences, University of East Anglia, Norwich NR4 7TJ, UK. (A.Ridgwell@uea.ac.uk)

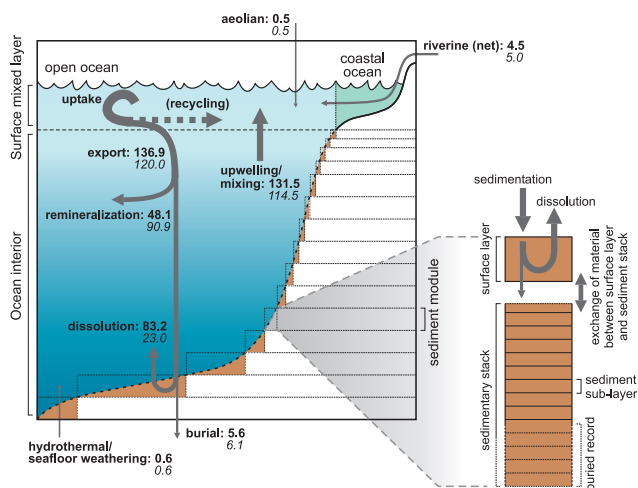


Figure 1. Schematic of the global ocean biogeochemical cycling of Si, together with the structure of the sediment system. Arrows indicate the flow of Si (as either silicic acid or biogenic opal), with values (in units of Tmol Si a^{-1}) of these fluxes in the model at steady state shown in bold, and contrasted with those shown in the work of *Tréguer et al.* [1995] (italics). The riverine input flux is quoted “less” removal in coastal/shelf zones (i.e., as the net input to the “open ocean”). The dotted arrow indicates recycling within the euphotic zone, not resolved in the simple export production scheme employed here. Indicated is the distribution of the 15 sediment modules (which together span 100–6000 m depth range of ocean) associated with each oceanic region in the zonally averaged representation of ocean circulation (see Figure 6). Each of these sediment modules is composed of a 10 cm thick surface layer (in which diagenesis is assumed to take place), underlain by a stack of (1 cm thick) storage or sediment compositional “memory” layers.